Strange mesons in nuclear matter at finite temperature

L. Tolós,[1] D. Cabrera,[2] and A. Ramos[3]

[1]*FIAS, Goethe-Universität Frankfurt am Main, Ruth-Moufang-Str. 1, D-60438 Frankfurt am Main, Germany*

[2]*Departamento de Física Teórica II, Universidad Complutense, E-28040 Madrid, Spain*

[3]*Departament d'Estructura i Constituents de la Matèria, Universitat de Barcelona, Diagonal 647, E-08028 Barcelona, Spain*

(Received 23 July 2008; published 17 October 2008)

We study the properties of K and $\bar{K}$ mesons in nuclear matter at finite temperature from a chiral unitary approach in coupled channels that incorporates the s and p waves of the kaon-nucleon interaction. The in-medium solution accounts for Pauli blocking effects, mean-field binding on all the baryons involved, and π and kaon self-energies. We calculate K and $\bar{K}$ (off-shell) spectral functions and single-particle properties. The $\bar{K}$ effective mass gets lowered by about -50 MeV in cold nuclear matter at saturation density and by half this reduction at $T = 100$ MeV. The p-wave contribution to the $\bar{K}$ optical potential, due to Λ, Σ, and Σ^* excitations, becomes significant for momenta larger than 200 MeV/c and reduces the attraction felt by the $\bar{K}$ in the nuclear medium. The $\bar{K}$ spectral function spreads over a wide range of energies, reflecting the melting of the $\Lambda(1405)$ resonance and the contribution of YN^{-1} components at finite temperature. In the KN sector, we find that the low-density theorem is a good approximation for the K self-energy close to saturation density due to the absence of resonance-hole excitations. The K potential shows a moderate repulsive behavior, whereas the quasiparticle peak is considerably broadened with increasing density and temperature. We discuss the implications for the decay of the ϕ meson at GSI Schwerionen Synchrotron energies as well as in the future Facility for Antiproton and Ion Research project.

DOI: 10.1103/PhysRevC.78.045205 PACS number(s): 13.75.Jz, 14.40.Aq, 21.65.−f, 25.80.Nv

I. INTRODUCTION

The properties of hadrons and, in particular, of mesons with strangeness in dense matter have been a matter of intense investigation over the past several years, in connection with the study of exotic atoms [1] and the analysis of heavy-ion collisions (HICs) [2,3].

At zero temperature, the study of the $\bar{K}$ interaction in nuclei has revealed some interesting characteristics. First, the presence below the $\bar{K}N$ threshold of the $\Lambda(1405)$ resonance gives rise to the failure of the $T\rho$ approximation for the $\bar{K}$ self-energy. Whereas the $\bar{K}N$ interaction is repulsive at threshold, the phenomenology of kaonic atoms requires an attractive potential. The consideration of Pauli blocking on the intermediate $\bar{K}N$ states [4,5] was found to shift the excitation energy of the $\Lambda(1405)$ to higher energies, hence changing the real part of the $\bar{K}N$ amplitude from repulsive in free space to attractive in a nuclear medium already at very low densities. Further steps were taken to account for self-consistency in the evaluation of the $\bar{K}$ self-energy [6,7] as well as for relevant medium effects on the intermediate meson-baryon states [8], which results in a moderate final size of the attractive potential as well as in a sizable imaginary part associated to several in-medium decay mechanisms [8–11]. Several studies of the $\bar{K}$ potential based on phenomenology of kaonic atoms have pointed toward a different class of deeply attractive potentials [12]. Unfortunately, the present experimental knowledge is unable to solve this controversy, as both kinds of potentials fairly describe the data from kaonic atoms [12,13].

A different direction in the study of this problem was given in Ref. [14], where a highly attractive antikaon-nucleus potential was constructed, leading to the prediction of narrow strongly bound states in few body systems [14–16]. This potential has been critically discussed in Ref. [17] because of the omission of the direct coupling of the $\pi\Sigma$ channel to itself, the assumption of the nominal $\Lambda(1405)$ as a single bound $\bar{K}$ state, the lack of self-consistency in the calculations and the seemingly too large nuclear densities obtained of around 10 times normal nuclear matter density at the center of the nucleus. Experiments devised to the observation of deeply bound kaonic states, measuring particles emitted after the absorption of K^- in several nuclei, reported signals that could actually be interpreted from conventional nuclear physics processes. The experimental observations could be explained simply either by the two-body absorption mechanism raised in Ref. [17], without [18–21] or with [22,23] final-state interactions, or coming from a three-body absorption process [24–26]. Actually, recent improved few-body calculations using realistic $\bar{K}N$ interactions and short-range correlations [27–30] predict few-nucleon kaonic states bound only by 50–80 MeV and having large widths of the order on 100 MeV, thereby disclaiming the findings of Refs. [14–16].

Relativistic heavy-ion experiments at beam energies below 2 AGeV [3,31,32] is another experimental scenario that has been testing the properties of strange mesons not only in a dense but also in a hot medium. Some interesting conclusions have been drawn comparing the different theoretical transport-model predictions and the experimental outcome on production cross sections, as well as energy and polar-angle distributions [3,31]. For example, despite the significantly different thresholds in binary NN collisions, there is a clear coupling between the K^- and K^+ yields because the K^- is predominantly produced via strangeness exchange from hyperons that, however, are created together with K^+ mesons. Furthermore, the K^- and K^+ mesons exhibit different freeze-out conditions as the K^- are continuously produced and

reabsorbed, leaving the reaction zone much later than the K^+ mesons. However, there is still not a consensus on the influence of the kaon-nucleus potential on those observables [33].

Compared to the $\bar{K}N$ interaction, the KN system has received comparatively less attention. Because of the lack of resonant states in the $S = +1$ sector, the single-particle potential of kaons has usually been calculated in a $T\rho$ approximation, with a repulsion of around 30 MeV for nuclear matter density (the information on T is taken from scattering lengths and energy dependence is ignored). However, a recent analysis of the KN interaction in the Jülich model has demonstrated that the self-consistency induces a significant difference in the optical potential with respect to the low-density approximation at saturation density, and the kaon potential exhibits a nontrivial momentum dependence [34].

A precise knowledge of kaon properties in a hot and dense medium is also an essential ingredient to study the fate of the ϕ meson. Electromagnetic decays of vector mesons offer a unique probe of high-density regions in nuclear production experiments and HICs [2]. The ϕ meson predominantly decays into $\bar{K}K$, which are produced practically at rest in the center-of-mass frame, each carrying approximately half of the mass of the vector meson. Such a system is highly sensitive to the available phase space, so that small changes in the kaon effective masses or the opening of alternative baryon-related decay channels may have a strong repercussion in the ϕ-meson mass and decay width. The analysis of the mass spectrum of the ϕ-decay products in dedicated experiments has drawn inconclusive results because the long-lived vector meson mostly decays out of the hot/dense system [35–40]. In addition, despite the sizable modifications predicted in most theoretical studies [41–48], the current experimental resolution typically dominates the observed spectrum from ϕ decays. Still, recent measurements of the ϕ transparency ratio in the nuclear photoproduction reaction by the LEPS Collaboration [38] have shed some light on the problem and seem to indicate an important renormalization of the absorptive part of the ϕ nuclear potential, as it was suggested in the theoretical analysis of Ref. [49]. The unprecedented precision achieved by the CERN NA60 Collaboration in the analysis of dimuon spectrum data from In-In collisions at 158 AGeV [50], as well as the advent of future studies of vector meson spectral functions to be carried out at the HADES [51] and CBM [52] experiments in the future Facility for Antiproton and Ion Research (FAIR), advise an extension of our current theoretical knowledge of the ϕ spectral function to the (μ_B, T) plane and, hence, of the K and $\bar{K}$ properties at finite temperature and baryon density.

In this work we evaluate the K and $\bar{K}$ self-energy, spectral function, and nuclear optical potentials in a nuclear medium at finite temperature. We follow the lines of Refs. [8,11,53,54] and build the s-wave KN and $\bar{K}N$ T matrices in a coupled-channels chiral unitary approach. Medium effects are incorporated by modifying the intermediate meson-baryon states. We account for Pauli blocking on intermediate nucleons, baryonic binding potentials, and meson self-energies for pions and kaons. The latter demands a self-consistent solution of the K and $\bar{K}$ self-energies as one sums the kaon nucleon scattering amplitude over the occupied states of the system, whereas the T matrix itself incorporates the information of the kaon self-energies in the intermediate meson-baryon Green's functions. The interaction in p wave is also accounted for in the form of YN^{-1} excitations, which lead to a sizable energy dependence of the $\bar{K}$ self-energy below the quasiparticle peak. Finite temperature calculations have been done in the Imaginary Time Formalism (ITF) to keep the required analytical properties of retarded Green's functions that, together with the use of relativistic dispersion relations for baryons (and, of course, for mesons), improves on some approximations typically used in former works. The organization of the present article goes as follows: in Sec. II we develop the formalism and ingredients on which the calculation is based. Section III is devoted to the presentation of the results. The $\bar{K}$ and K self-energies and spectral functions are discussed in Secs. III A and III B, respectively. We devote Sec. III C to the discussion of momentum, density, and temperature dependence of $\bar{K}$ and K nuclear optical potentials. Finally, in Sec. IV we draw our conclusions as well as the implications of the in-medium properties of kaons at finite temperature in transport calculations and ϕ-meson phenomenology. We also give final remarks pertaining to the present and future works.

II. KAON NUCLEON SCATTERING IN HOT NUCLEAR MATTER

In this section we discuss the evaluation of the effective kaon nucleon scattering amplitude in a dense nuclear medium, extending the unitarized chiral model for $\bar{K}$ of Refs. [8,11] to account for finite temperature. This allows us to obtain the in-medium K and $\bar{K}$ self-energy, spectral function, and nuclear optical potential. We follow closely the lines of Ref. [53], where a similar study was reported for open-charm mesons in hot nuclear matter.

A. s-wave kaon nucleon scattering and kaon self-energy

The kaon nucleon interaction at low energies is successfully described in chiral perturbation theory (χPT) [55–59]. The lowest-order chiral Lagrangian that couples the octet of light pseudoscalar mesons to the octet of $1/2^+$ baryons is given by

$$\mathcal{L}_1^{(B)} = \langle \bar{B} i\gamma^\mu \nabla_\mu B\rangle - M\langle \bar{B}B\rangle + \tfrac{1}{2}D\langle \bar{B}\gamma^\mu\gamma_5\{u_\mu, B\}\rangle + \tfrac{1}{2}F\langle \bar{B}\gamma^\mu\gamma_5[u_\mu, B]\rangle, \quad (1)$$

where B is the SU(3) matrix for baryons, M is the baryon mass, u contains the Φ matrix of mesons, and the symbol $\langle\ \rangle$ denotes the flavor trace. The SU(3) matrices appearing in Eq. (1) are standard in notation and can be found, for instance, in Ref. [54]. The axial-vector coupling constants have been determined in Ref. [60] and read $D = 0.8$ and $F = 0.46$.

Keeping at the level of two meson fields, the covariant derivative term in Eq. (1) provides the following interaction Lagrangian in s wave,

$$\mathcal{L}_1^{(B)} = \left\langle \bar{B} i\gamma^\mu \frac{1}{4f^2}[(\Phi\partial_\mu\Phi - \partial_\mu\Phi\Phi)B - B(\Phi\partial_\mu\Phi - \partial_\mu\Phi\Phi)]\right\rangle. \quad (2)$$

Expanding the baryon spinors and vertices in M_B^{-1} the following expression of the s-wave kaon nucleon tree-level amplitude can be derived

$$V_{ij}^s = -C_{ij}\frac{1}{4f^2}\left(2\sqrt{s} - M_{B_i} - M_{B_j}\right) \times \left(\frac{M_{B_i}+E_i}{2M_{B_i}}\right)^{1/2}\left(\frac{M_{B_j}+E_j}{2M_{B_j}}\right)^{1/2}, \quad (3)$$

with M_{B_i} and E_i the mass and energy of the baryon in the ith channel, respectively. The coefficients C_{ij} form a symmetric matrix and are given in Ref. [54]. The meson decay constant f in the s-wave amplitude is taken as $f = 1.15 f_\pi$. This renormalized value provides a satisfactory description of experimental low-energy $\bar{K}N$ scattering observables [such as cross sections and the properties of the $\Lambda(1405)$ resonance] using only the interaction from the lowest-order chiral Lagrangian plus unitarity in coupled channels. We consider the following channels in the calculation of the scattering amplitude: in the strangeness sector $S = -1$ we have $\bar{K}N, \pi\Sigma, \eta\Lambda$, and $K\Xi$ for isospin $I = 0$; $\bar{K}N, \pi\Lambda, \pi\Sigma, \eta\Sigma$, and $K\Xi$ for $I = 1$. For $S = 1$, there is only one single channel, KN, for each isospin.

In Refs. [8,11,54] unitarization of the tree-level amplitudes in coupled channels was implemented, which extends the applicability of χPT to higher energies and in particular allows us to account for dynamically generated resonances. In particular, the $\Lambda(1405)$ shows up in the unitarized s-wave $\bar{K}N$ amplitude. Following Ref. [54], the effective kaon nucleon scattering amplitude is obtained by solving the Bethe-Salpeter equation in coupled channels (in matrix notation),

$$T = V + \overline{VGT}, \quad (4)$$

where we use the s-wave tree-level amplitudes as the potential (kernel) of the equation, V_{ij}^s, and

$$G_i(\sqrt{s}) = \mathrm{i}\int \frac{d^4q}{(2\pi)^4}\frac{M_i}{E_i(-\vec{q})}\frac{1}{\sqrt{s} - q_0 - E_i(-\vec{q}) + \mathrm{i}\varepsilon} \times \frac{1}{q_0^2 - \vec{q}^{\,2} - m_i^2 + \mathrm{i}\varepsilon} \quad (5)$$

stands for the intermediate two-particle meson-baryon Green's function of channel i (G is diagonal). In principle, both V and T enter off-shell in the momentum integration ($\overline{VGT}$ term) of the meson-baryon loop. However, as it was shown in Refs. [11,54], the (divergent) off-shell contributions of V and T in the s-wave interaction can be reabsorbed in a renormalization of the bare coupling constants and masses order by order. Therefore, both V and T can be factorized on-shell out of the meson-baryon loop, leaving the four-momentum integration only in the two-particle meson-baryon propagators. An alternative justification of solving the Bethe-Salpether equation with on-shell amplitudes may be found in the framework of the N/D method, applied for meson-meson interactions in Ref. [61] and for meson-baryon interactions in Ref. [62]. We are thus left with a set of linear algebraic equations with trivial solution,

$$T = [1 - VG]^{-1}V. \quad (6)$$

The meson-baryon loop function, G_i, needs to be regularized. We apply a cutoff in the three-momentum of the intermediate particles, which provides a simple and transparent regularization method for in-medium calculations, cf. Refs. [8,11].

To obtain the effective s-wave $\bar{K}(K)N$ amplitude in hot and dense matter, we incorporate in the loop functions the modifications on the properties of the mesons and baryons induced by temperature and density.

In the ITF, the baryon propagator in a hot medium is given by:

$$\mathcal{G}_B(\omega_m, \vec{p}; T) = \frac{1}{\mathrm{i}\omega_m - E_B(\vec{p}, T)}, \quad (7)$$

where $\mathrm{i}\omega_m = \mathrm{i}(2m+1)\pi T + \mu_B$ is the fermionic Matsubara frequency, with μ_B the baryon chemical potential, and E_B is the baryon single-particle energy, which, in the case of nucleons and singly strange hyperons, will also contain the medium binding effects obtained within a temperature-dependent Walecka-type σ-ω model (see Ref. [63]). According to this model, the nucleon energy spectrum in mean-field approximation is obtained from

$$E_N(\vec{p}, T) = \sqrt{\vec{p}^{\,2} + M_N^*(T)^2} + \Sigma^v, \quad (8)$$

with the vector potential Σ^v and the effective mass $M_N^*(T)$ given by

$$\Sigma^v = \left(\frac{g_v}{m_v}\right)^2 \rho \qquad M_N^*(T) = M_N - \Sigma^s, \quad \text{with} \quad \Sigma^s = \left(\frac{g_s}{m_s}\right)^2 \rho_s, \quad (9)$$

where m_s and m_v are the meson masses ($m_s = 440$ MeV, $m_v = 782$ MeV), whereas g_s and g_v are the scalar and vector density-dependent coupling constants. These constants are obtained by reproducing the energy per particle of symmetric nuclear matter at $T = 0$ coming from a Dirac-Brueckner-Hartree-Fock calculation (see Table 10.9 of Ref. [64]). The vector (ρ) and scalar (ρ_s) densities are obtained by momentum integration, namely

$$\rho_{(s)} = 4\int \frac{d^3p}{(2\pi)^3} n_N^{(s)}(\vec{p}, T), \quad (10)$$

of the corresponding vector $[n_N(\vec{p}, T)]$ and scalar $[n_N^s(\vec{p}, T)]$ density distributions, which are defined in terms of the nucleon Fermi-Dirac function as

$$n_N(\vec{p}, T) = \frac{1}{1 + \exp\{[E_N(\vec{p}, T) - \mu_B]/T\}} \quad (11)$$

and

$$n_N^s(\vec{p}, T) = \frac{M_N^*(T) n_N(\vec{p}, T)}{\sqrt{\vec{p}^{\,2} + M_N^*(T)^2}}, \quad (12)$$

respectively. The quantities $E_N(\vec{p}, T)$, $M_N^*(T)$, and μ_B are obtained simultaneously and self-consistently for given ρ and T and for the corresponding values of g_s and g_v.

The hyperon masses and energy spectra,

$$E_Y(\vec{p}, T) = \sqrt{\vec{p}^{\,2} + M_Y^*(T)^2} + \Sigma_Y^v, \quad (13)$$

TABLE I. σ-ω model at finite temperature.

ρ(fm^{-3})	T (MeV)	μ_B (MeV)	M_N^* (MeV)	Σ^v (MeV)	M_Λ^* (MeV)	Σ_Λ^v (MeV)	M_Σ^* (MeV)	Σ_Σ^v (MeV)
0.0425	0	920	781	121	1010	81	1088	81
0.0425	50	820	793	121	1019	81	1096	81
0.0425	100	618	805	121	1026	81	1104	81
0.0425	150	364	815	121	1033	81	1110	81
0.17	0	920	579	282	872	188	950	188
0.17	50	892	605	282	893	188	970	188
0.17	100	783	634	282	913	188	990	188
0.17	150	618	659	282	929	188	1006	188
0.34	0	979	443	422	787	281	865	281
0.34	50	969	470	422	803	281	881	281
0.34	100	905	510	422	830	281	907	281
0.34	150	787	545	422	853	281	930	281

can be easily inferred from those for the nucleon as

$$\Sigma_Y^v = \frac{g_v^Y g_v}{m_v^2}\rho = \frac{2}{3}\left(\frac{g_v}{m_v}\right)^2\rho = \frac{2}{3}\Sigma^v,$$

$$M_Y^*(T) = M_Y - \Sigma_Y^s = M_Y - \frac{g_s^Y g_s}{m_s^2}\rho_s = M_Y - \frac{2}{3}\left(\frac{g_s}{m_s}\right)^2\rho_s$$

$$= M_Y - \frac{2}{3}[M_N - M_N^*(T)]. \quad (14)$$

Here we have assumed that the σ and ω fields couple only to the u and d quarks, as in Refs. [65,66], so the scalar and vector coupling constants for hyperons and charmed baryons are

$$g_v^Y = \tfrac{2}{3}g_v, \quad g_s^Y = \tfrac{2}{3}g_s. \quad (15)$$

In this way, the potential for hyperons follows the simple light quark counting rule as compared with the nucleon potential: $V_Y = 2/3V_N$. As reference, we quote in Table I the nucleon and hyperon single-particle properties for three densities ($0.25\rho_0$, ρ_0, and $2\rho_0$), where $\rho_0 = 0.17$ fm^{-3} is the normal nuclear matter saturation density, and four temperatures ($T =$ 0, 50, 100, and 150 MeV). The hyperon attraction at $\rho = \rho_0$ and $T = 0$ MeV is about -50 MeV, the size of which gets reduced as temperature increases turning even into repulsion, especially at higher densities. This behavior results from the fact that the temperature-independent vector potential takes over the strongly temperature-dependent scalar potential that decreases with temperature. We note that the quark-meson coupling (QMC) calculations of Refs. [65,66], performed at $T = 0$, obtained a somewhat smaller scalar potential (about half the present one) for the Λ and Σ baryons due to the inclusion of nonlinear terms associated to quark dynamics. To the best of our knowledge, no temperature effects have been studied within this framework.

The meson propagator in a hot medium is given by

$$D_M(\omega_n, \vec{q}; T) = \frac{1}{(\mathrm{i}\omega_n)^2 - \vec{q}^{\,2} - m_M^2 - \Pi_M(\omega_n, \vec{q}; T)}, \quad (16)$$

where $\mathrm{i}\omega_n = \mathrm{i}2n\pi T$ is the bosonic Matsubara frequency and $\Pi_M(\omega_n, \vec{q}; T)$ is the meson self-energy. Note that throughout this work we set the mesonic chemical potential to zero, because we are dealing with an isospin symmetric nuclear medium with zero strangeness. We will consider in this work the dressing of pions and kaons.

An evaluation of the in-medium self-energy for pions at finite temperature and baryonic density was given in the Appendix of Ref. [10], which generalized the zero-temperature evaluation of the pion self-energy from Refs. [67,68] by incorporating thermal effects. We recall that the pion self-energy in nuclear matter at $T = 0$ is strongly dominated by the p-wave coupling to particle-hole (ph) and Δ-hole (Δh) components (a small, repulsive s-wave contribution takes over at small momenta), as well as to 2p-2h excitations, which account for pion absorption processes, and short-range correlations. We come back to the pion self-energy in Sec. II C, where we improve on some approximations in previous works.

In the case of the kaons, the self-energy receives contributions of comparable size from both s- and p-wave interactions with the baryons in the medium. We evaluate the s-wave self-energy from the effective $\bar{K}(K)N$-scattering amplitude in the medium, a procedure that, as will be shown explicitly in the following, must be carried out self-consistently. The p-wave part of the kaon self-energy will be discussed separately in the next section.

The evaluation of the effective $\bar{K}(K)N$ s-wave scattering amplitude in the hot medium proceeds by first obtaining the meson-baryon two-particle propagator function (meson-baryon loop) at finite temperature in the ITF, $\mathcal{G}_{\mathrm{MB}}$. Given the analytical structure of $\mathcal{G}_{\mathrm{MB}}$ it is convenient to use the spectral (Lehmann) representation for the meson propagator,

$$D_M(\omega_n, \vec{q}; T) = \int d\omega\, \frac{S_M(\omega, \vec{q}; T)}{\mathrm{i}\omega_n - \omega}$$

$$= \int_0^\infty d\omega\, \frac{S_M(\omega, \vec{q}; T)}{\mathrm{i}\omega_n - \omega} - \int_0^\infty d\omega\, \frac{S_{\bar{M}}(\omega, \vec{q}; T)}{\mathrm{i}\omega_n + \omega}, \quad (17)$$

where S_M, $S_{\bar{M}}$ stand for the spectral functions of the meson and its corresponding anti-particle. The separation in the

second line of Eq. (17) reflects the retarded character of the meson self-energy and propagator, $\mathrm{Im}\Pi(-q_0,\vec{q};T) = -\mathrm{Im}\Pi(q_0,\vec{q};T)$. Due to strangeness conservation, K and $\bar{K}$ experience markedly different interactions in a nuclear medium [8], which justifies using a different notation $(S_M, S_{\bar{M}})$ for the spectral functions in Eq. (17).[1] Combining Eqs. (16) and (17), conveniently continued analytically from the Matsubara frequencies onto the real energy axis, one can write

$$S_M(\omega,\vec{q};T) = -\frac{1}{\pi}\mathrm{Im}D_M(\omega,\vec{q};T) = -\frac{1}{\pi}\frac{\mathrm{Im}\Pi_M(\omega,\vec{q};T)}{|\omega^2-\vec{q}^{\,2}-m_M^2-\Pi_M(\omega,\vec{q};T)|^2}. \quad (18)$$

Applying the finite-temperature Feynman rules, the meson-baryon loop function in the ITF reads

$$\mathcal{G}_{\mathrm{MB}}(W_m,\vec{P};T) = -T\int\frac{d^3q}{(2\pi)^3}\sum_n\frac{1}{\mathrm{i}W_m-\mathrm{i}\omega_n-E_B(\vec{P}-\vec{q},T)} \times\int_0^\infty d\omega\left[\frac{S_M(\omega,\vec{q};T)}{\mathrm{i}\omega_n-\omega}-\frac{S_{\bar{M}}(\omega,\vec{q};T)}{\mathrm{i}\omega_n+\omega}\right], \quad (19)$$

where $\vec{P}$ is the external total three-momentum and W_m an external fermionic frequency, $\mathrm{i}W_m = \mathrm{i}(2m+1)\pi T+\mu_B$. Note that we follow a quasirelativistic description of baryon fields all throughout this work: in Eq. (19) the negative energy part of the baryon propagator has been neglected but we use relativistic dispersion relations. All the Dirac structure is included in the definition of the tree-level amplitudes. The Matsubara sums can be performed using standard complex analysis techniques for each of the two terms in the meson propagator and one finds

$$\mathcal{G}_{\mathrm{MB}}(W_m,\vec{P};T) = \int\frac{d^3q}{(2\pi)^3}\int_0^\infty d\omega \times\left[S_M(\omega,\vec{q};T)\frac{1-n_B(\vec{P}-\vec{q},T)+f(\omega,T)}{\mathrm{i}W_m-\omega-E_B(\vec{P}-\vec{q},T)} + S_{\bar{M}}(\omega,\vec{q};T)\frac{n_B(\vec{P}-\vec{q},T)+f(\omega,T)}{\mathrm{i}W_m+\omega-E_B(\vec{P}-\vec{q},T)}\right], \quad (20)$$

with $f(\omega,T) = [\exp(\omega/T)-1]^{-1}$ the meson Bose distribution function at temperature T. The former expression can be analytically continued onto the real energy axis, $G_{\mathrm{MB}}(P_0+\mathrm{i}\varepsilon,\vec{P};T) = \mathcal{G}_{\mathrm{MB}}(\mathrm{i}W_m\to P_0+\mathrm{i}\varepsilon,\vec{P};T)$, cf. Eq. (20). With these medium modifications the meson-baryon retarded propagator at finite temperature (and density) reads

$$G_{\bar{K}(K)N}(P_0+\mathrm{i}\varepsilon,\vec{P};T) = \int\frac{d^3q}{(2\pi)^3}\frac{M_N}{E_N(\vec{P}-\vec{q},T)}\left[\int_0^\infty d\omega S_{\bar{K}(K)}(\omega,\vec{q};T) \times\frac{1-n_N(\vec{P}-\vec{q},T)}{P_0+\mathrm{i}\varepsilon-\omega-E_N(\vec{P}-\vec{q},T)} + \int_0^\infty d\omega S_{K(\bar{K})}(\omega,\vec{q};T) \times\frac{n_N(\vec{P}-\vec{q},T)}{P_0+\mathrm{i}\varepsilon+\omega-E_N(\vec{P}-\vec{q},T)}\right], \quad (21)$$

for $\bar{K}(K)N$ states and

$$G_{\pi Y}(P_0+\mathrm{i}\varepsilon,\vec{P};T) = \int\frac{d^3q}{(2\pi)^3}\frac{M_Y}{E_Y(\vec{P}-\vec{q},T)}\int_0^\infty d\omega S_\pi(\omega,\vec{q},T) \times\left[\frac{1+f(\omega,T)}{P_0+\mathrm{i}\varepsilon-\omega-E_Y(\vec{P}-\vec{q},T)} + \frac{f(\omega,T)}{P_0+\mathrm{i}\varepsilon+\omega-E_Y(\vec{P}-\vec{q},T)}\right] \quad (22)$$

for $\pi\Lambda$ or $\pi\Sigma$ states, where $P=(P_0,\vec{P})$ is the total two-particle momentum and $\vec{q}$ is the meson three-momentum in the nuclear medium rest frame. Note that for consistency with the free space meson-baryon propagator, given in Eq. (5), we have included the normalization factor M_B/E_B in the baryon propagator. We have explicitly written the temperature dependence of the baryon energies indicating that we account for mean-field binding potentials as discussed above. The second term in the $\bar{K}N$ loop function typically provides a small, real contribution for the energy range in P_0 we are interested in. To simplify the numerical evaluation of the self-consistent $\bar{K}N$ amplitude we replace $S_K(\omega,\vec{q};T)$ by a free-space δ function in Eq. (21). This approximation is sensible as long as the K spectral function in the medium still peaks at the quasiparticle energy and the latter does not differ much from the energy in vacuum, as we will confirm in Sec. III. In Eq. (21) we neglected the kaon distribution function, because we expect Bose enhancement to be relevant only for the lightest meson species in the range of temperatures explored in the present study, $T = 0$–150 MeV.

The πY loop function, in particular, incorporates the $1+f(\omega,T)$ enhancement factor that accounts for the contribution from thermal pions at finite temperature, cf. Eq. (22). In this case, we have neglected the fermion distribution for the participating hyperons, which is a reasonable approximation for the range of temperature and baryonic chemical potential that we have studied (cf. Table I).

In the case of $\eta\Lambda$, $\eta\Sigma$, and $K\Xi$ intermediate states, we simply consider the meson propagator in free space and include only the effective baryon energies modified by the mean-field

[1] In the case of pions, for instance, in an isospin symmetric nuclear medium, all the members of the isospin triplet $(\pi^\pm,\pi^0)$ acquire the same self-energy and one can write $S_\pi(-q_0,\vec{q};T) = -S_\pi(q_0,\vec{q};T)$ with the subsequent simplification of Eq. (17).

binding potential, namely

$$G_l(P_0+\mathrm{i}\varepsilon,\vec{P};T)=\int\frac{d^3q}{(2\pi)^3}\,\frac{1}{2\omega_l(\vec{q})}\,\frac{M_l}{E_l(\vec{P}-\vec{q},T)}\times\frac{1}{P_0+\mathrm{i}\varepsilon-\omega_l(\vec{q})-E_l(\vec{P}-\vec{q},T)}. \tag{23}$$

The latter channels are less relevant in the unitarization procedure of the s-wave scattering amplitude. They are important to maintain SU(3) symmetry through using a complete basis of states in the coupled-channels procedure, as well as for producing a better description of branching ratios between the various scattering transitions at threshold. However, the width and position of the $\Lambda(1405)$ are basically determined from the unitarized coupling of $\bar{K}N$ and $\pi\Sigma$ channels [54]. In addition, the changes that kaons [34,69] and η mesons [70,71] experience in the medium at moderate densities are comparably weaker than for π and $\bar{K}$, which justifies the simplification adopted here.

As mentioned above, all meson-baryon loop functions in our approach are regularized with a cutoff in the three-momentum integration, $q_{\max}$. We adopt here the regularization scale that was set in Ref. [54], where the $\bar{K}N$-scattering amplitude was evaluated in free space, leading to a remarkable description of several $\bar{K}N$-scattering observables and the dynamical generation of the $\Lambda(1405)$ resonance with a single parameter, $q_{\max}=630$ MeV/c.

Finally, we obtain the in-medium s-wave $\bar{K}(K)$ self-energy by integrating $T_{\bar{K}(K)N}$ over the nucleon Fermi distribution at a given temperature,

$$\Pi^s_{\bar{K}(K)}(q_0,\vec{q};T)=\int\frac{d^3p}{(2\pi)^3}\,n_N(\vec{p},T)\big[T^{(I=0)}_{\bar{K}(K)N}(P_0,\vec{P};T)+3T^{(I=1)}_{\bar{K}(K)N}(P_0,\vec{P};T)\big], \tag{24}$$

where $P_0=q_0+E_N(\vec{p},T)$ and $\vec{P}=\vec{q}+\vec{p}$ are the total energy and momentum of the $\bar{K}(K)N$ pair in the nuclear medium rest frame and q stands for the momentum of the $\bar{K}(K)$ meson also in this frame. The kaon self-energy must be determined self-consistently because it is obtained from the in-medium amplitude, $T_{\bar{K}(K)N}$, which requires the evaluation of the $\bar{K}(K)N$ loop function, $G_{\bar{K}(K)N}$, and the latter itself is a function of $\Pi_{\bar{K}(K)}(q_0,\vec{q};T)$ through the kaon spectral function, cf. Eqs. (18) and (21). Note that Eq. (24) is strictly valid in cold nuclear matter. In the Appendix B we provide a derivation of the s-wave self-energy from the kaon nucleon T-matrix in ITF and give arguments for the validity of Eq. (24) as a sensible approximation at moderate temperatures.

B. p-wave kaon self-energy

The main contribution to the p-wave kaon self-energy comes from the Λ and Σ pole terms, which are obtained from the axial-vector couplings in the Lagrangian [D and F terms in Eq. (1)]. The $\Sigma^*(1385)$ pole term is also included explicitly with couplings to the kaon-nucleon states that were evaluated from SU(6) symmetry arguments in Ref. [45].

In Ref. [11], the combined s- and p-wave $\bar{K}$ self-energy was obtained self-consistently in cold nuclear matter by unitarizing the tree-level amplitudes in both channels. Unitarization of the p-wave channel, however, did not provide dramatic effects over the tree-level pole terms. Those were used in Ref. [45] to evaluate the p-wave self-energy. The latter is built up from hyperon-hole (Yh) excitations and it provides sizable strength in the $\bar{K}$ spectral function below the quasiparticle peak and a moderate repulsion (as it is expected from the excitation of subthreshold resonances) at nuclear matter density. Medium effects and unitarization actually move the position of the baryon pole with respect to that in free space [11]. We incorporate this behavior here in an effective way through the use of baryon mean-field potentials and re-evaluate the relevant many-body diagrams for the p-wave self-energy at finite temperature and density, which considerably simplifies the numerical task. We shall work in the ITF, improving on some approximations of former evaluations [10,45,46]. Hence, the total K and $\bar{K}$ self-energy will consist of the sum of the s- and p-wave contributions described here and in the former section. Note that the p-wave self-energy enters the self-consistent calculation of the s-wave self-energy as the K and $\bar{K}$-meson propagators in the intermediate states on the s-wave kaon-nucleon amplitude are dressed with the total self-energy at each iteration.

We can write the $\bar{K}$ p-wave self-energy as the sum of each of the Yh contributions,

$$\Pi^p_{\bar{K}}(q_0,\vec{q};T)=\tfrac{1}{2}\tilde{V}^2_{\bar{K}N\Lambda}\vec{q}^{\,2}f^2_\Lambda(q_0,\vec{q})U_{\Lambda N^{-1}}(q_0,\vec{q};T)+\tfrac{3}{2}\tilde{V}^2_{\bar{K}N\Sigma}\vec{q}^{\,2}f^2_\Sigma(q_0,\vec{q})U_{\Sigma N^{-1}}(q_0,\vec{q};T)+\tfrac{1}{2}\tilde{V}^2_{\bar{K}N\Sigma^*}\vec{q}^{\,2}f^2_{\Sigma^*}(q_0,\vec{q})U_{\Sigma^* N^{-1}}(q_0,\vec{q};T), \tag{25}$$

where U_Y stands for the YN^{-1} Lindhard function at finite temperature and baryonic density, and $\tilde{V}^2_{\bar{K}NY}$ represents the $\bar{K}NY$ coupling from the chiral Lagrangian in a nonrelativistic approximation (leading order in a M_B^{-1} expansion) and includes the required isospin multiplicity. They can be found, for instance, in Ref. [45]. The f_Y factors account for relativistic recoil corrections to the $\bar{K}NY$ vertices, which improve on the lowest-order approximation and still allow us to write the self-energy in a simple form, where all the dynamical information from the p-wave coupling is factorized out of the momentum sum in the fermionic loop. These factors read

$$f^2_{\Lambda,\Sigma}(q_0,\vec{q})=[2M_{\Lambda,\Sigma}+2q_0(M_{\Lambda,\Sigma}-M_N)-(q_0)^2+\vec{q}^{\,2}+2M_NE_{\Lambda,\Sigma}(\vec{q})]/4M_NE_{\Lambda,\Sigma}(\vec{q}),$$
$$f^2_{\Sigma^*}(q_0,\vec{q})=(1-q_0/M_{\Sigma^*})^2. \tag{26}$$

We have also accounted for the finite size of the vertices by incorporating phenomenological hadronic form factors of dipole type via the replacement $\vec{q}^{\,2}\to F_K(\vec{q}^{\,2})\vec{q}^{\,2}$ with $F_K(\vec{q}^{\,2})=[\Lambda_K^2/(\Lambda_K^2+\vec{q}^{\,2})]^2$, where $\Lambda_K=1050$ MeV. We provide explicit expressions for $U_{YN^{-1}}$ in Appendix A.

In Refs. [45,46] the K and $\bar{K}$ self-energy in p wave was obtained for cold nuclear matter, and it was extended to the finite temperature case in Ref. [10]. We present here a comparison of our results for different approximations as the

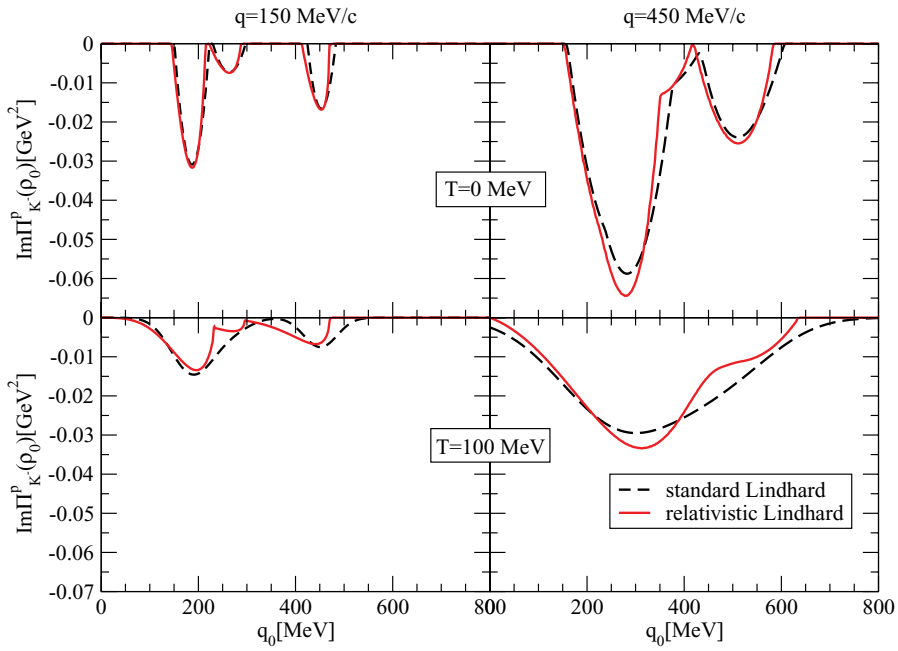

FIG. 1. (Color online) Imaginary part of the $\bar{K}$ p-wave self-energy from different evaluations of the YN^{-1} Lindhard function (see text) at $\rho = \rho_0$. The upper panels correspond to $T = 0$, whereas in the lower panels $T = 100$ MeV.

ones used in former evaluations, particularly in the $T \to 0$ limit. In Fig. 1 we present the imaginary part of the $\bar{K}$ p-wave self-energy as a function of the kaon energy, evaluated at nuclear matter density and two different kaon momenta. In the upper panels the dashed lines have been obtained by using, in Eq. (25), the standard nonrelativistic evaluation of the YN^{-1} Lindhard function [45,46], the analytical expression of which is also quoted in Appendix A. The solid lines correspond to our calculation in Eq. (A3) for $T = 0$ MeV. Both results agree quite well, which ensures that our calculation has the correct $T \to 0$ limit. The observed differences, particularly the threshold energies at which each YN^{-1} component is open/closed, are related to the use of nonrelativistic baryon energies (in dashed lines) and some further approximations that we discuss below.

At $T = 100$ MeV (lower panels), the dashed lines correspond to the evaluation of the Lindhard function in Ref. [10], which extends the zero-temperature, nonrelativistic calculation by replacing the nucleon occupation number, $\theta(p_F - p)$, by the corresponding Fermi-Dirac distribution, $n_N(\vec{p}, T)$. Note that, in our result (solid lines), the Matsubara sum automatically generates a nonvanishing term proportional to the hyperon distribution function, cf. Eqs. (A1) and (A3) in Appendix A. Despite the absence of a crossed kinematics mechanism (as for instance in ph and Δh excitations for pions) this guarantees that the imaginary part of the $\bar{K}$ self-energy identically vanishes at zero energy ($q_0 = 0$) as it follows from the (retarded) crossing property of the thermal self-energy, $\mathrm{Im}\Pi^p_{\bar{K}}(-q_0, \vec{q}; T) = -\mathrm{Im}\Pi^p_K(q_0, \vec{q}; T)$.[2] The two calculations at $T = 100$ MeV exhibit some nontrivial differences. In the finite-T extension of the nonrelativistic result the YN^{-1} structures and thresholds are more diluted and the Σ component is not resolved even at low momentum, whereas in the relativistic result the three components are clearly identifiable at $q = 150$ MeV/c. In both calculations the strength of the imaginary part extends to lower energies so that the energy gap in cold nuclear matter is absent here. However, as mentioned, the relativistic calculation in the ITF vanishes exactly at $q_0 = 0$, whereas the nonrelativistic, finite-T extended result does not. In addition, the standard nonrelativistic calculations (at $T = 0$ and finite T) [10,45,46] omit $\vec{p}^{\,2}$ terms proportional to $(M_Y^{-1} - M_N^{-1})$ in the energy balance of the two-particle propagator, which are responsible for cutting the available YN^{-1} phase space for high external energies (q_0). As a consequence, the dashed lines in the lower panels exhibit a high-energy tail that is attenuated by the nucleon distribution, whereas the relativistic result has a clear (temperature dependent) end point. This happens for each of the excited hyperon components independently and it is particularly visible for the Σ^*. The Λ and Σ tails mix with each other and are responsible for the washing out of the Σ structure at high momentum values.

Finally, the K p-wave self-energy can be obtained following the same procedure as above. The excitation mechanisms in this case correspond exactly to the crossed kinematics of those of the $\bar{K}$. Taking advantage of the crossing property of the thermal self-energy, we obtain the K self-energy from the $\bar{K}$ one replacing $q_0 \to -q_0$ in $\Pi^p_{\bar{K}}(q_0, \vec{q}; T)$ (modulo a sign flip in the imaginary part). The crossed kinematics causes the YN^{-1} excitations to be far off-shell. In cold nuclear matter, for instance, Π^p_K is real and mildly attractive. At finite temperature, though, the fermion distributions of the nucleon and hyperon can accommodate low-energy (off-shell) kaons and Π^p_K receives a small imaginary part that rapidly decays with increasing energy.

[2] At zero energy ($q_0 = 0$) the K and $\bar{K}$ modes cannot be distinguished and thus $\mathrm{Im}\,\Pi^p_{\bar{K}}(0, \vec{q}; T) = -\mathrm{Im}\Pi^p_K(0, \vec{q}; T) \equiv 0$. This is accomplished exactly in Eq. (A3) in Appendix A for $q_0 = 0$.

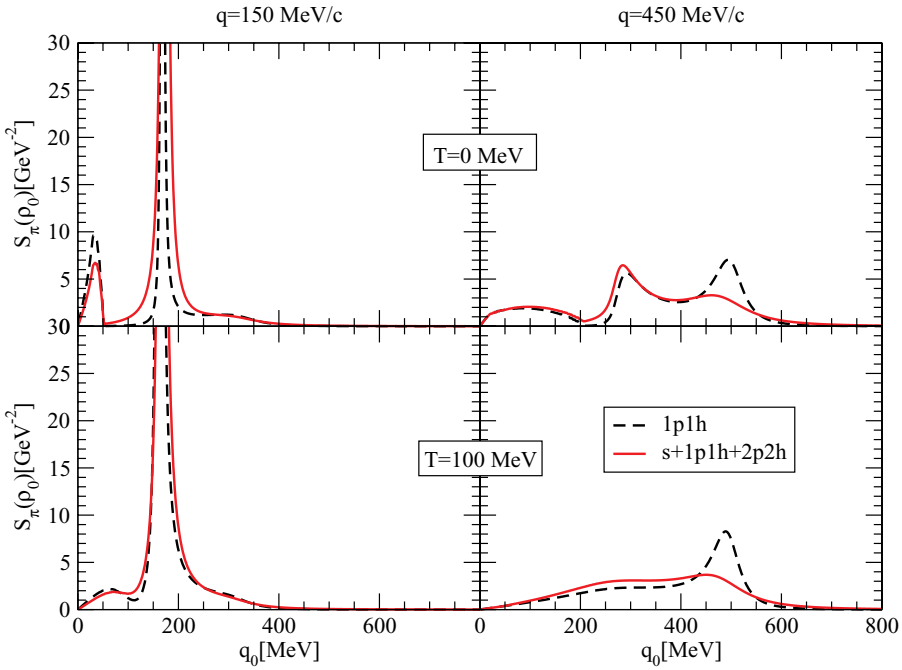

FIG. 2. (Color online) Pion spectral function at $\rho = \rho_0$ for two different momenta and temperatures, $T = 0$ (upper panels) and $T = 100$ MeV (lower panels). The dashed lines correspond to the p-wave self-energy calculation, including ph, Δh, and short-range correlations. The solid lines include, in addition, the (small) s-wave self-energy and the 2p2h absorption mechanisms.

C. Pion self-energy

We briefly discuss here the relevant many-body mechanisms that modify the pion propagator, which enters the evaluation of the in-medium $\bar{K}N$ amplitude, cf. Eqs. (6) and (22). In cold nuclear matter, the pion spectral function exhibits a mixture of the pion quasiparticle mode and ph, Δh excitations [67]. The meson-baryon chiral Lagrangian in Eq. (1) provides the πNN p-wave vertex, whereas the $\pi N\Delta$ vertex can be determined from the standard nonrelativistic derivation of the Raritta-Schwinger interaction Lagrangian. However, we shall use phenomenological πNN and $\pi N\Delta$ coupling constants determined from analysis of pion nucleon and pion nucleus reactions. Their values are $f_N/m_\pi = 0.007244$ MeV^{-1} and $f_\Delta/f_N = 2.13$. The lowest-order p-wave pion self-energy due to ph and Δh excitations then reads

$$\Pi^p_{\pi NN^{-1}+\pi\Delta N^{-1}}(q_0,\vec{q};T) = \left(\frac{f_N}{m_\pi}\right)^2 \vec{q}^{\,2}[U_{NN^{-1}}(q_0,\vec{q};T) + U_{\Delta N^{-1}}(q_0,\vec{q};T)], \quad (27)$$

where the finite temperature Lindhard functions for the ph and Δh excitations are given in Appendix A. Note that, for convenience, we have absorbed the $\pi N\Delta$ coupling in the definition of $U_{\Delta N^{-1}}$.

The strength of the considered collective modes is modified by repulsive, spin-isospin NN and $N\Delta$ short-range correlations [72], which we include in a phenomenological way with a single Landau-Migdal interaction parameter, $g' = 0.7$. The RPA-summed pion self-energy then reads

$$\Pi^p_\pi(q_0,\vec{q};T) = \frac{\left(\frac{f_N}{m_\pi}\right)^2 F_\pi(\vec{q}^{\,2})\vec{q}^{\,2}\,[U_{NN^{-1}}(q_0,\vec{q};T) + U_{\Delta N^{-1}}(q_0,\vec{q};T)]}{1 - \left(\frac{f_N}{m_\pi}\right)^2 g'[U_{NN^{-1}}(q_0,\vec{q};T) + U_{\Delta N^{-1}}(q_0,\vec{q};T)]}, \quad (28)$$

which also contains the effect of the same monopole form factor at each πNN and $\pi N\Delta$ vertex as used in $T = 0$ studies, namely $F_\pi(\vec{q}^{\,2}) = (\Lambda_\pi^2 - m_\pi^2)/[\Lambda_\pi^2 - (q_0)^2 + \vec{q}^{\,2}]$, with $\Lambda_\pi = 1200$ MeV, as is needed in the empirical study of NN interactions. Finally, for consistence with former evaluations of the pion self-energy, we have also accounted for one-body s-wave scattering and 2p2h mechanisms, following the results in Refs. [68,73,74], which we have kept to be the same as in $T = 0$.

In Fig. 2 we show the pion spectral function at normal nuclear matter density for two different momenta. At $T = 0$ (upper panels) one can easily distinguish the different modes populating the spectral function. At low momentum, the pion quasiparticle peak carries most of the strength together with the ph structure at lower energies. The Δh mode starts to manifest to the right-hand side of the pion quasiparticle peak. Note that the pion mode feels a sizable attraction with respect to that in free space. At higher momentum, the excitation of the Δ is clearly visible and provides a considerable amount of strength that mixes with the pion mode. As a consequence, the latter broadens considerably. The solid lines include also the contributions from the pion s-wave self-energy and two-body absorption. These mechanisms, especially the latter, generate a background of strength that further broadens the spectral function, softening in particular the pion peak at low momentum and the Δ excitation at higher momentum.

The lower panels correspond to a temperature of $T = 100$ MeV. The softening of the nucleon occupation number due to thermal motion causes a broadening of the three modes present in the spectral function. At $q = 450$ MeV, the ph, Δh, and pion peaks are completely mixed, although some distinctive strength still prevails at the Δh excitation energy. The s-wave and 2p2h self-energy terms completely wash out the structures that were still visible at zero temperature. For higher temperatures we have checked that no further structures can be resolved in the spectral function, in agreement with

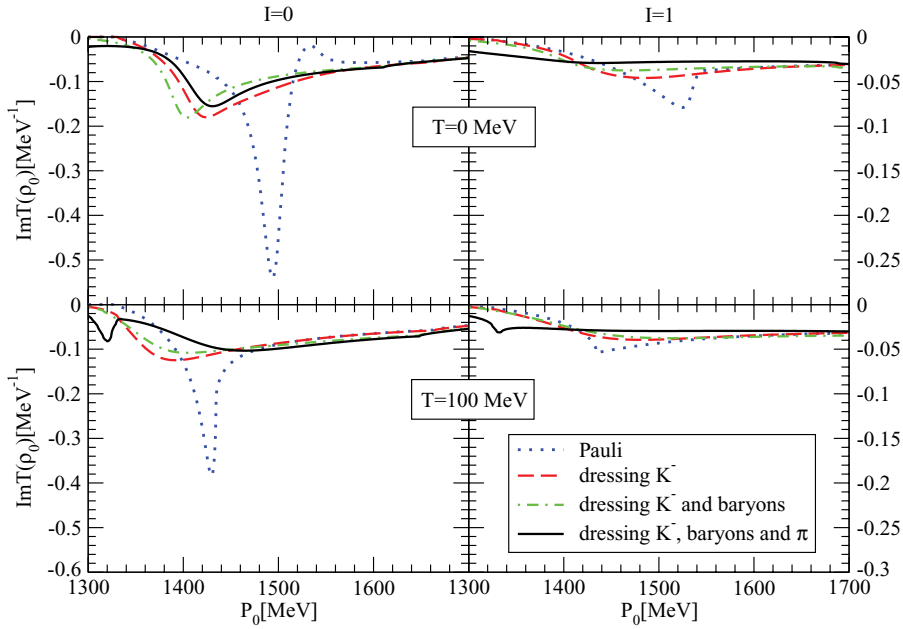

FIG. 3. (Color online) Imaginary part of the in-medium $\bar{K}N$ s-wave amplitude for $I = 0$ and $I = 1$ at ρ_0 as a function of the center-of-mass energy P_0, for $T = 0$, 100 MeV, and for the different approaches discussed in the text.

Ref. [75]. We, however, find differences at the numerical level, as we expected, because we have implemented different hadronic form factors and Landau-Migdal interactions in our model. Moreover, to keep closer to phenomenology, we have also implemented in our model the energy-dependent p-wave decay width of the Δ, which favors mixing of the Δh excitation with the pion mode.

III. RESULTS AND DISCUSSION

A. The $\bar{K}$ meson spectral function in a hot nuclear medium

We start this section by showing in Fig. 3 the s-wave $\bar{K}N$ amplitude for $I = 0$ and $I = 1$ as a function of the center-of-mass energy, P_0, calculated at nuclear matter density, ρ_0, and temperatures $T = 0$ MeV (first row) and $T = 100$ MeV (second row). We have considered four different in-medium approaches: a first iteration that includes only Pauli blocking on the nucleon intermediate states (dotted lines) and three other self-consistent calculations of the $\bar{K}$ meson self-energy increasing gradually the degree of complexity: one includes the dressing of the $\bar{K}$ meson (long-dashed lines), another considers in addition the mean-field binding of the baryons in the various intermediate states (dot-dashed lines), and, finally, the complete model that includes also the pion self-energy (solid lines). Recall that the $I = 0$ amplitude is governed by the behavior of the dynamically generated $\Lambda(1405)$ resonance.

We start commenting on the $T = 0$ results shown in the upper panels, where we clearly see that the inclusion of Pauli blocking on the intermediate nucleon states generates the $I = 0$ $\Lambda(1405)$ at higher energies than its position in free space. This has been discussed extensively in the literature [4,6,8–11] and it is due to the restriction of available phase space in the unitarization procedure. The self-consistent incorporation of the attractive $\bar{K}$ self-energy moves the $\Lambda(1405)$ back in energy, closer to the free position, whereas it gets diluted due to the opening of the $\Lambda(1405)N \to \pi N\Lambda, \pi N\Sigma$ decay modes [6,8,10,11]. The inclusion of baryon binding has mild effects, lowering slightly the position of the resonance peak. A similar smoothing behavior is observed for the $I = 1$ amplitude as we include medium modifications on the intermediate meson-baryon states. As already pointed out in Refs. [8,10,11], when pions are dressed new channels are available, such as ΛNN^{-1} or ΣNN^{-1} (and similarly with ΔN^{-1} components), so the $\Lambda(1405)$ gets further diluted.

At a finite temperature of 100 MeV (lower panels), the $\Lambda(1405)$ resonance gets diluted and is produced, in general, at lower energies due to the smearing of the Fermi surface that reduces the Pauli blocking effects. When pions are dressed the strongly diluted resonance moves slightly to higher energies compared to the zero-temperature case. The cusplike structures that appear at the lower energy side signal the opening of the $\pi\Sigma$ threshold on top of the already opened YNN^{-1} one. Note that the cusplike structure appears enhanced in the $I = 0$ case. We believe that this is a manifestation at finite temperature and density of the two-pole structure of the $\Lambda(1405)$. As seen in Refs. [60,62,76–78], this resonance is, in fact, the combination of two poles in the complex plane that appear close in energy and couple strongly to either $\bar{K}N$ or $\pi\Sigma$ states. These two poles move apart and can be even resolved in a hot medium because density and temperature influence each of them differently. Although not shown in the figure, we find that, at twice nuclear matter density, the pole that couples more strongly to $\pi\Sigma$ states moves further below the $\pi\Sigma$ threshold and acquires a clear Breit-Wigner shape. This allows us to conclude that the cusp observed in the $I = 0$ amplitude at $T = 100$ MeV and $\rho = \rho_0$ is essentially a reflection of this pole. The shape of the corresponding resonance appears distorted with respect to a usual Breit-Wigner because the pole lies just below the threshold of the $\pi\Sigma$ channel to which it couples very strongly, a behavior known as Flatté effect [79]. Note that these structures are not seen in the $T = 0$ results because the $\pi\Sigma$ threshold in that case is located at around 1295 MeV, out of the range of the plot.

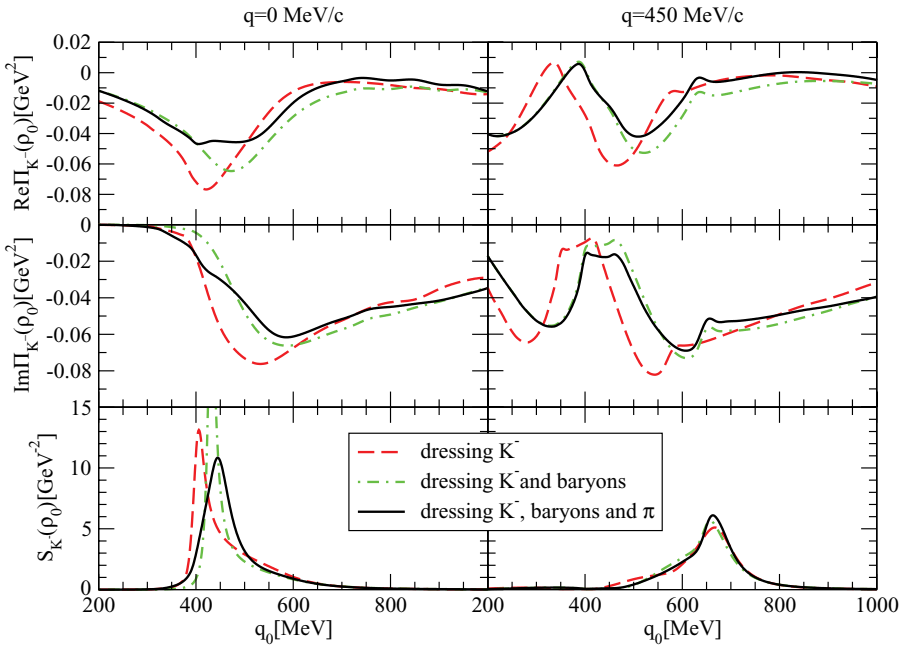

FIG. 4. (Color online) Real and imaginary parts of the $\bar{K}$ self-energy and spectral density, as functions of the $\bar{K}$ energy, for $q = 0$ MeV/c and $q = 450$ MeV/c. Results have been obtained at $T = 0$ and ρ_0, including $(s + p)$-wave contributions, for the three self-consistent approaches discussed in the text.

Results for the $\bar{K}$ self-energy and spectral function at ρ_0 and $T = 0$, including s- and p-wave contributions, obtained in the different self-consistent approaches are compared in Fig. 4. At $q = 0$ MeV/c, the inclusion of the baryon binding potential (dot-dashed lines) moves the quasiparticle peak of the spectral function, which is defined as

$$E_{qp}(\vec{q})^2 = \vec{q}^2 + m_{\bar{K}}^2 + \mathrm{Re}\,\Pi_{\bar{K}}(E_{qp}(\vec{q}), \vec{q}), \qquad (29)$$

to higher energies with respect to the case with no binding (dashed lines). The pion dressing (solid lines) further alters the behavior of the self-energy and, hence, that of the spectral function. The attraction of the antikaon mode decreases, whereas its width increases due to the opening of new decay channels induced by the ph and Δh pion excitations. At finite momentum, the p-wave ΛN^{-1}, ΣN^{-1}, and $\Sigma^* N^{-1}$ excitation modes are clearly visible in the self-energy around 300, 400, and 600 MeV, respectively. The latter mode mixes very strongly with the quasiparticle peak, making the differences between various self-consistent approaches to be less visible in the $\bar{K}$ spectral function. Similar results were obtained in Ref. [11]. The differences between both $T = 0$ calculations arise mainly by the use in this work of different (and more realistic) baryon binding potentials. The effects of the particular details of the nucleon spectrum on the $\bar{K}$ spectral function have been noted recently in the $T = 0$ study of Ref. [80].

The effect of finite temperature on the different partial-wave contributions to the $\bar{K}$ self-energy is shown in Fig. 5. In this figure we display the real and imaginary parts of the $\bar{K}$ self-energy together with the $\bar{K}$ spectral function for the self-consistent approximation that dresses baryons and includes the pion self-energy. We show the results as a function of the $\bar{K}$ energy for two different momenta, $q = 0$ MeV/c (left column) and $q = 450$ MeV/c (right column). The different curves correspond to $T = 0$ and $T = 100$ MeV, including the s-wave and the $(s + p)$-wave contributions.

According to Eq. (25), the present model does not give an explicit p-wave contribution to the $\bar{K}$ self-energy at zero momentum. The small differences between the s and the $s + p$ calculations observed at $q = 0$ MeV/c are due to the indirect effects of having included the p-wave self-energy in the intermediate meson-baryon loop. The importance of the p-wave self-energy is more evident at a finite momentum of $q = 450$ MeV/c. The effect of the subthreshold ΛN^{-1}, ΣN^{-1}, and $\Sigma^* N^{-1}$ excitations is repulsive at the $\bar{K}N$ threshold. This repulsion together with the strength below threshold induced by the those excitations can be easily seen in the spectral function at finite momentum (third row). The quasiparticle peak moves to higher energies while the spectral function falls off slowly on the left-hand side.

Temperature results in a softening of the real and imaginary part of the self-energy as the Fermi surface is smeared out. The peak of the spectral function moves closer to the free position while it extends over a wider range of energies.

For completeness, we show in Fig. 6 the evolution of the $\bar{K}$ spectral function with increasing temperature for two different densities, ρ_0 (upper row) and $2\rho_0$ (lower row), and two momenta, $q = 0$ MeV/c (left column) and $q = 450$ MeV/c (right column), in the case of the full self-consistent calculation that includes the dressing of baryons and the pion self-energy. At $q = 0$ MeV/c the quasiparticle peak moves to higher energies with increasing temperature due to the loss of strength of the attractive effective $\bar{K}N$ interaction. Furthermore, the quasiparticle peak enhances its collisional broadening and gets mixed with the strength associated to the $\Lambda(1405)$ appearing both to the right (slow fall out) and left (cusp-like structures) of the peak. All these effects are less pronounced at a finite momentum of $q = 450$ MeV/c. In this case, the region of the quasiparticle peak is exploring $\bar{K}$ energies of around 700 MeV, where the self-energy has a weaker energy dependence with temperature, as seen in Fig. 5. We note that, as opposed to the zero-momentum case, the width of the quasiparticle peak

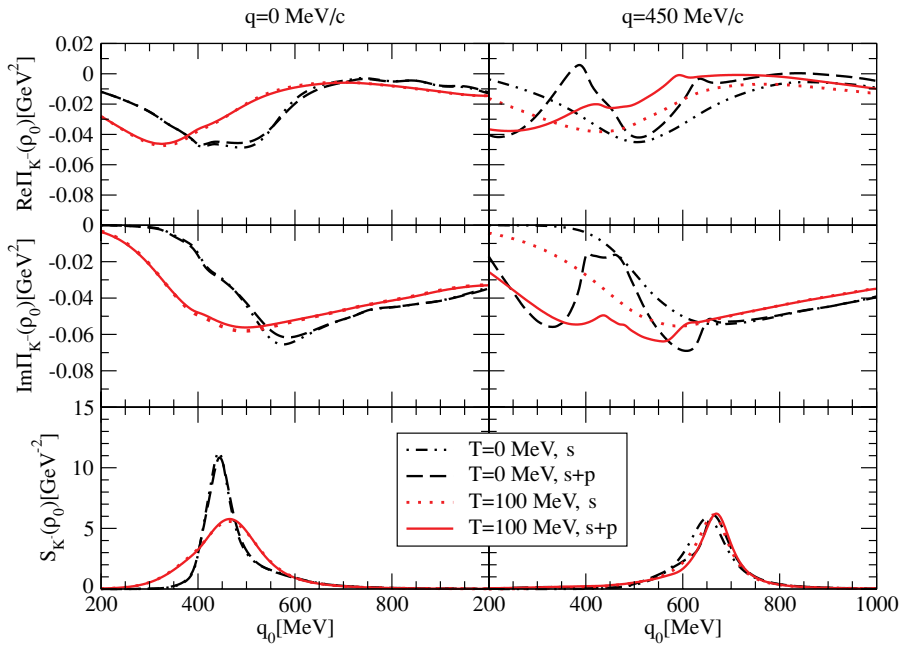

FIG. 5. (Color online) Real and imaginary parts of the $\bar{K}$ self-energy and spectral function at ρ_0, for $q = 0$, 450 MeV/c and $T = 0, 100$ MeV, as function of the $\bar{K}$ energy, including s- and $(s + p)$-wave contributions in the full self-consistent calculation.

decreases with increasing temperature because of the reduction of the intermixing with the $\Sigma^* N^{-1}$ excitations that get diluted in a hot medium. As for the density effects, we just note that the quasiparticle peaks widens for larger nuclear density due to the enhancement of collision and absorption processes. In fact, a significant amount of strength is visible at energy values substantially below the quasiparticle peak. The fact that the $\bar{K}$ spectral function spreads to lower energies, even at finite momentum, may have relevant implications on the phenomenology of the ϕ-meson propagation and decay in a nuclear medium. We will further elaborate on this point in the Conclusions section.

B. *K* meson in nuclear matter at finite temperature

The evolution with temperature and density of the properties of kaons is also a matter of high interest. In particular, kaons are ideal probes to test the high-density phase of relativistic heavy-ion collisions at incident energies ranging from 0.6 to 2 AGeV and for studying the stiffness of the nuclear equation of state [3,31]. Moreover, there is a strong interconnection between the K^+, K^-, and ϕ channels, which can lead to important changes in the ϕ-meson production in heavy-ion collisions [81].

In the $S = 1$ sector, only the KN channel is available and, hence, the many-body dynamics of the K meson in nuclear

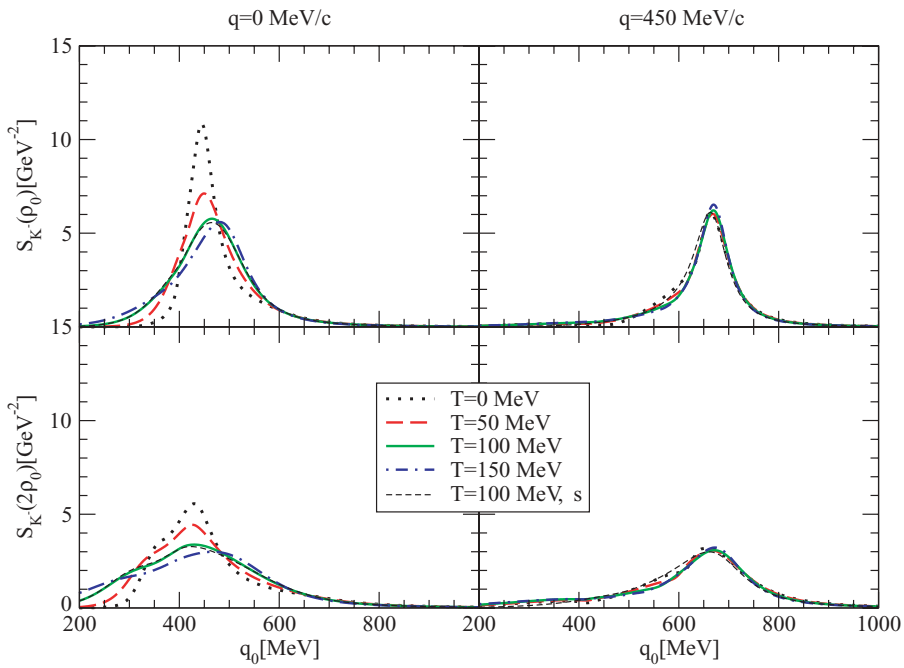

FIG. 6. (Color online) The $\bar{K}$ meson spectral function for $q = 0$ MeV/c and $q = 450$ MeV/c at ρ_0 and $2\rho_0$ as a function of the $\bar{K}$ meson energy for different temperatures and for the self-consistent calculation including the dressing of baryons and pions.

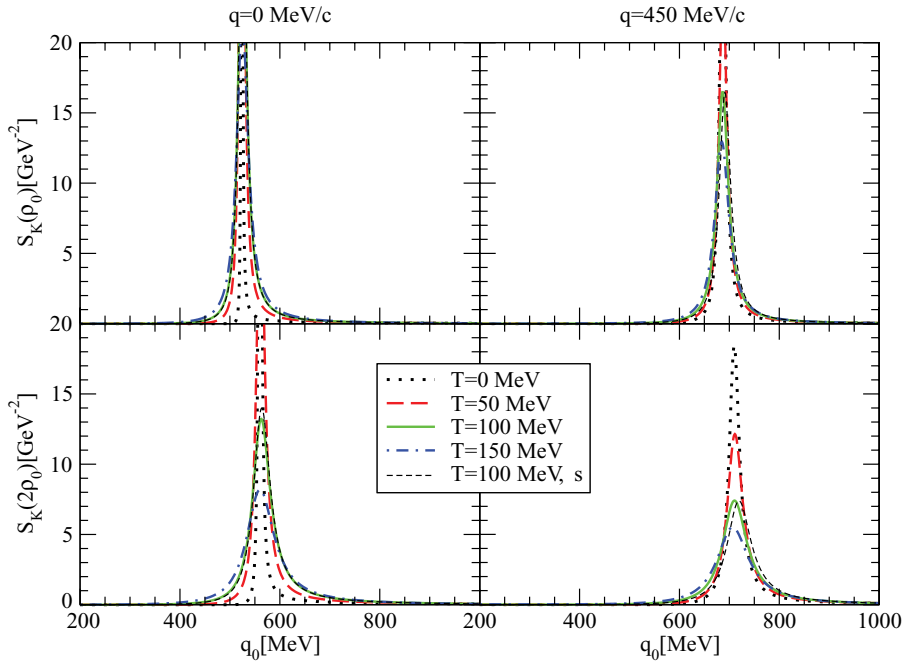

FIG. 7. (Color online) The K-meson spectral function for $q = 0$ MeV/c and $q = 450$ MeV/c at ρ_0 and $2\rho_0$ as a function of the K-meson energy for different temperatures.

medium is simplified with respect to the $\bar{K}N$ case. The K spectral function at $q = 0$ and $q = 450$ MeV/c is displayed in Fig. 7 for the self-consistent calculation that includes the dressing of baryons for ρ_0 (upper row) and $2\,\rho_0$ (lower row) and different temperatures. The K meson is described by a narrow quasiparticle peak that dilutes with temperature and density as the phase space for collisional KN states increases. The s-wave self-energy provides a moderate repulsion at the quasiparticle energy, which translates into a shift of the K spectral function to higher energies with increasing density. In contrast to the $\bar{K}N$ case, the inclusion of p waves has a mild effect on the kaon self-energy (compare thin-dashed lines to solid lines at $T = 100$ MeV and $q = 450$ MeV/c), as they arise from far off-shell YN^{-1} excitations in crossed kinematics. These excitations provide a small, attractive, and barely energy-dependent contribution to the K self-energy.

We can define the K optical potential in the nuclear medium as

$$U_K(\vec{q}, T) = \frac{\Pi_K(E_{qp}(\vec{q}), \vec{q}, T)}{2\sqrt{m_K^2 + \vec{q}^{\,2}}}, \tag{30}$$

which, at zero momentum, can be identified as the in-medium shift of the K meson mass. The K mass shift obtained in the self-consistent calculation that considers also the nucleon binding effects is displayed in Fig. 8 as a function of the nuclear density for $T = 0$ MeV. Our self-consistent results are compared to those of the low-density or $T\rho$ approximation, obtained by replacing the medium-dependent amplitude by the free-space one in Eq. (24). We observe that the kaon potential at nuclear saturation density in the $T\rho$ approximation is 4 MeV less repulsive than in the case of the self-consistent approach, which gives a repulsion of 29 MeV. This value is in qualitative agreement with other self-consistent calculations [34,82] and close to the 20 MeV of repulsion obtained in K^+ production on nuclei by the ANKE experiment of the COSY Collaboration [83]. We conclude that the low-density theorem for densities below normal nuclear matter is fulfilled within 15% due to the smooth energy dependence of the KN interaction tied to the absence of resonant states close to the KN threshold.

C. In-medium $\bar{K}$ and K optical potentials at finite temperature

In this last subsection we provide the K and $\bar{K}$ optical potentials at conditions reached in heavy-ion collisions for beam energies of the order or less than 2 AGeV, where temperatures can reach values of $T = 100$ MeV together with densities up to a few times normal nuclear density [3,31,32].

In Figs. 9 and 10, we show the $\bar{K}$ and K optical potentials at $T = 100$ MeV for different densities ($0.25\rho_0$, ρ_0, and $2\rho_0$), including s (dotted lines) and $(s + p)$ waves (solid lines), as

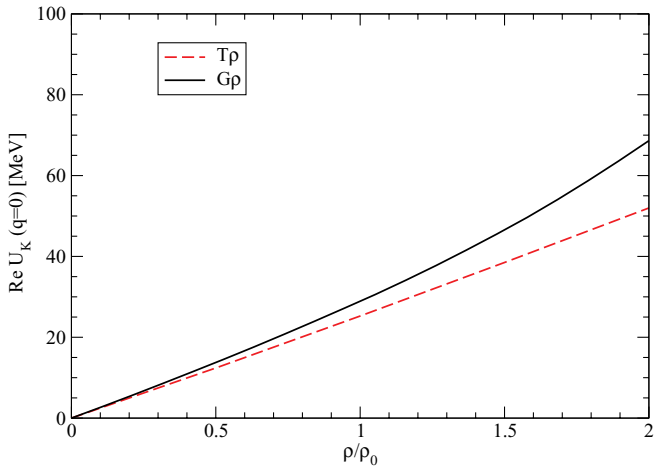

FIG. 8. (Color online) The K mass shift for $T = 0$ MeV as a function of density, obtained within the self-consistent calculation and in the $T\rho$ approximation.

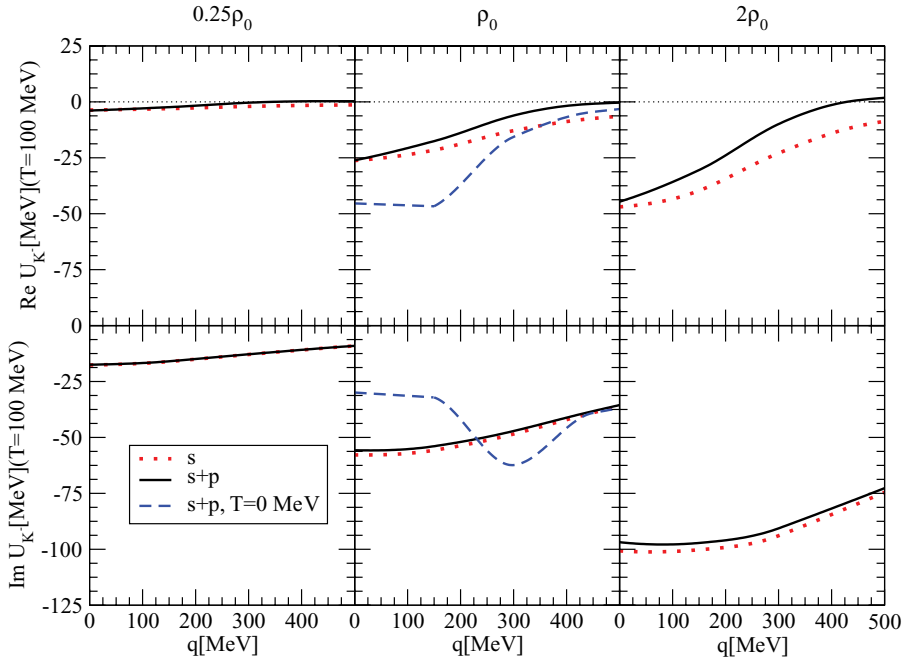

FIG. 9. (Color online) The $\bar{K}$ potential for the full self-consistent calculation at $T = 100$ MeV and $0.25\rho_0$, ρ_0, and $2\rho_0$ as a function of momentum. The $\bar{K}$ potential at $T = 0$ and ρ_0, including $(s + p)$ waves, is also shown.

functions of the meson momentum. In the case of ρ_0, we also show the potential at $T = 0$ including $(s + p)$ waves (dashed lines).

The real part of the $\bar{K}$ potential becomes more attractive as we increase the density, going from -4 MeV at $0.25\rho_0$ to -45 MeV at $2\rho_0$ for $q = 0$, when both s and p waves are included. The repulsive p-wave contributions to the $\bar{K}$ potential become larger as density increases, reducing substantially the amount of attraction felt by the $\bar{K}$. Compared to a previous self-consistent calculation using the Jülich meson-exchange model [9,10], here we observe a stronger dependence of the optical potential with the $\bar{K}$ momentum.

The imaginary part of the $\bar{K}$ optical potential at $T = 100$ MeV is little affected by p waves, which, as seen in Fig. 5, basically modify the $\bar{K}$ self-energy below the quasiparticle peak. The imaginary part of the potential shows a flat behavior at low momentum and, eventually, its magnitude decreases with increasing momentum as the quasiparticle energy moves away from the region of YN^{-1} excitations.

With respect to the zero temperature case, shown for ρ_0 in the middle panels of Fig. 9, the optical potential at $T = 100$ MeV shows less structure. The real part amounts to basically half the attraction obtained at $T = 0$ MeV, whereas the imaginary part gets enhanced at low momentum, due to the

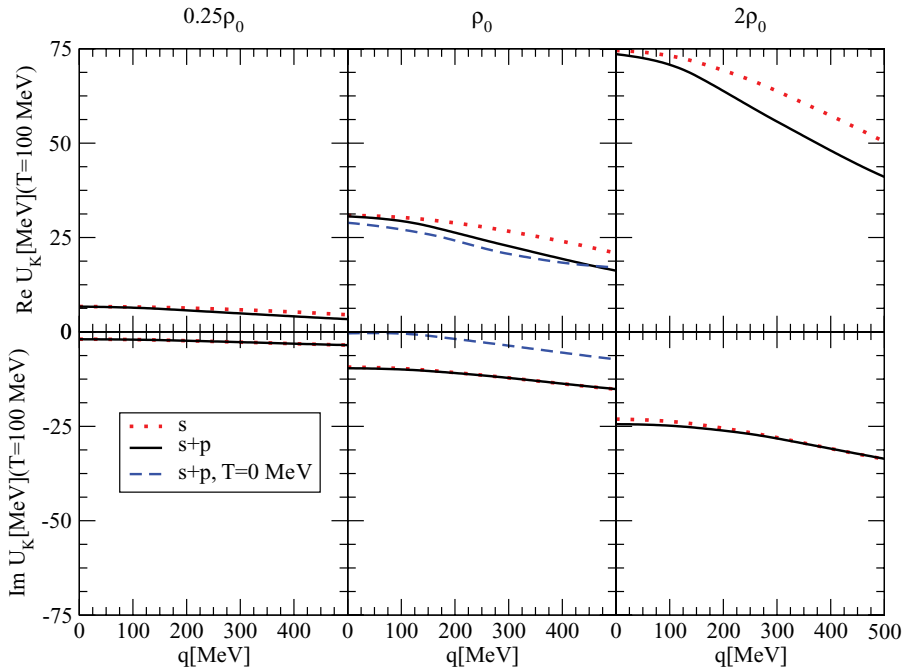

FIG. 10. (Color online) The K potential for the full self-consistent calculation at $T = 100$ MeV and $0.25\rho_0$, ρ_0, and $2\rho_0$ as a function of momentum. The K potential at $T = 0$ and ρ_0, including $(s + p)$ waves, is also shown.

increase of collisional width, and reduced at high momentum, due to the decoupling of the $\bar{K}$ quasiparticle mode from the $\Sigma^* N^{-1}$ one.

As seen in Fig. 10, the K-meson potential changes from 7 MeV at $0.25\rho_0$ to 74 MeV at $2\rho_0$ for $q = 0$ MeV/c and receives its major contribution from the s-wave interaction, the p wave providing a moderately attractive correction. The imaginary part moves from -2 MeV at $0.25\rho_0$ to -25 MeV at $2\rho_0$ for $q = 0$ MeV/c and its magnitude grows moderately with increasing momentum as the available phase space also increases.

Finite temperature affects the real part of the K-meson potential mildly, as can be seen for ρ_0 from comparing the dashed and solid lines in the middle panels of Fig. 10. The magnitude of the imaginary part increases with temperature for all momenta, consistently with the increase of thermically excited nucleon states.

From our results for $\bar{K}$ and K mesons, it is clear that p-wave effects can be neglected at subnuclear densities at the level of the quasiparticle properties. However, they become substantially important as density increases and are also responsible for a considerable amount of the strength at low energies in the spectral function.

IV. SUMMARY, CONCLUSIONS, AND OUTLOOK

We have obtained the $\bar{K}$ and K self-energies in symmetric nuclear matter at finite temperature from a chiral unitary approach, which incorporates the s and p waves of the kaon-nucleon interaction. At tree level, the s-wave amplitude is obtained from the Weinberg-Tomozawa term of the chiral Lagrangian. Unitarization in coupled channels is imposed by solving the Bethe-Salpeter equation with on-shell amplitudes. The model generates dynamically the $\Lambda(1405)$ resonance in the $I = 0$ channel. The in-medium solution of the s-wave amplitude, which proceeds by a re-evaluation of the meson-baryon loop function, accounts for Pauli-blocking effects, mean-field binding on the nucleons and hyperons via a temperature-dependent σ-ω model, and the dressing of the pion and kaon through their corresponding self-energies. This requires a self-consistent evaluation of the K and $\bar{K}$ self-energies. The p-wave self-energy is accounted for through the corresponding hyperon-hole ($Y N^{-1}$) excitations. Finite temperature expressions have been obtained in the ITF, giving a formal justification of some approximations typically done in the literature and, in some cases, improving on the results of previous works. For instance, in this formalism, the Lindhard function of $Y N^{-1}$ excitations automatically accounts for Pauli blocking on the thermally excited hyperons and satisfies the analytical constraints of a retarded self-energy.

The $\bar{K}$ self-energy and, hence, its spectral function show a strong mixing between the quasiparticle peak and the $\Lambda(1405)N^{-1}$ and $Y N^{-1}$ excitations. The effect of the p-wave $Y N^{-1}$ subthreshold excitations is repulsive for the $\bar{K}$ potential, compensating in part the attraction provided by the s-wave $\bar{K}N$ interaction. Temperature softens the p-wave changes on the spectral function at the quasiparticle energy. Together with the s-wave mechanisms, the p-wave self-energy provides a low-energy tail that spreads the spectral function considerably, due to the smearing of the Fermi surface for nucleons. Similarly, the size of the imaginary part of the potential decreases with momentum, as the $\bar{K}$ mode decouples from subthreshold absorption mechanisms.

The narrow K spectral function dilutes with density and temperature as the number of collisional KN states is increased. A moderate repulsion, coming from the dominant s-wave self-energy, moves the quasiparticle peak to higher energies in the hot and dense medium. The absence of resonant states close to threshold validates the use of the low-density theorem for the K optical potential approximately up to saturation density. The inclusion of p waves has a mild attractive effect on the K self-energy and potential, which results from $Y N^{-1}$ excitations in crossed kinematics.

The properties of strange mesons at finite temperature for densities of 2–3 times normal nuclear matter have been object of intensive research in the context of relativistic heavy-ion collisions at beam energies below 2 AGeV [3,31]. The comparison between the experimental results on production cross sections, energy distributions, and polar angle distributions and the different transport-model calculations has lead to several important conclusions, such as the coupling between the K^- and the K^+ yields by strangeness exchange and the fact that the K^+ and K^- mesons exhibit different freeze-out conditions. However, there is still debate on the influence of the kaon-nucleus potential on those observables. The in-medium modifications of the $\bar{K}$ and K properties devised in this article could be used in transport calculations and tested against the data from the current experimental programs in heavy ions [3,31,32].

The fact that the $\bar{K}$ spectral function spreads to low energies, even at finite momentum, may have relevant implications on the phenomenology of the ϕ-meson propagation and decay in a nuclear medium. The reduced phase space for the dominant decay channel in vacuum, $\phi \to \bar{K}K$, makes the ϕ-meson decay width a sensitive probe of kaon properties in a hot and dense medium (the p-wave nature of the $\phi\bar{K}K$ coupling further enhances this sensitivity). In Refs. [45,46] the ϕ-meson mass and decay width in nuclear matter were studied from a calculation of the $\bar{K}$ and K self-energies in a chiral unitary framework similar to the present work (the most relevant differences and novelties introduced in this work have been discussed in previous sections). The overall attraction of the $\bar{K}$ meson together with a sizable broadening of its spectral function [which reflects the fate of the $\Lambda(1405)$ in a nuclear medium], induced a remarkable increase of Γ_ϕ of almost one order of magnitude at $\rho = \rho_0$ as compared to the width in free space, as several decay mechanisms open in the medium such as $\phi N \to KY$ and $\phi N \to K\pi Y$. The LEPS Collaboration [38] has confirmed that the ϕ-meson width undergoes strong modifications in the medium from the study of the inclusive nuclear ϕ photoproduction reaction on different nuclei. The observed effects even surpass the sizable modifications obtained in Refs. [45,46] and predicted for the ϕ photoproduction reaction in Ref. [49].

At finite temperature (CERN-SPS, GSI-SIS, and GSI-FAIR conditions), despite the $\bar{K}$ peak return toward its free position, we expect a similar or even stronger broadening of the

ϕ meson, as the $\bar{K}$ spectral function further dilutes in the medium effectively increasing the available phase space. Note, in addition, that the presence of thermally excited mesons induces "stimulated" $\phi \to \bar{K}K$ decays (as well as diffusion processes) [84,85]. Since Bose enhancement is more effective on the lighter modes of the system, the low-energy tail of the $\bar{K}$ spectral function may contribute substantially to the ϕ decay width.

At RHIC and LHC conditions, the hot medium is expected to have lower net baryonic composition. One may conclude, as a consequence, that the contribution from interactions with baryons will be smaller. The relevance of baryonic density effects even at high temperatures has been stressed for the ρ and ϕ meson clouds in hot and dense matter [2,47,86]. In the case of $\phi \to \bar{K}K$ decays, a finite density of antibaryons allows the K to interact with the medium through the charge-conjugated mechanisms described here for the $\bar{K}$ and vice versa (in the limit of $\mu_B = 0$ the $\bar{K}$ and K self-energies are identical). At small net baryon density, whereas the effective contribution from the real parts of the $K, \bar{K}$ self-energies tend to vanish, it is not the case for the imaginary parts, which are always cumulative. Thus even at small baryonic chemical potential, the presence of antibaryons makes up for the loss of reactivity from having smaller nuclear densities. Additionally, the relevance of kaon interactions with the mesonic gas (ignored in this work) becomes manifest in this regime, as it has been pointed out in Refs. [48,87–89]. These mechanisms, together with Bose enhancement of $\bar{K}K$ decays, point toward a sizable increase of the ϕ reactivity even at very high temperatures.

Therefore, we plan to study the influence of the $\bar{K}K$ cloud on the properties of the ϕ meson in a nuclear medium at finite temperature [90], extending our previous analysis for cold nuclear matter [45,46,49]. Such changes on the ϕ-meson properties are a matter of interest in the current and future experimental heavy-ion programs [32,51,52]. In particular, the future FAIR facility at GSI will devote special attention to the in-medium vector meson spectral functions. The HADES experiment will operate at higher beam energy of the order of 8–10 AGeV, providing complementary information on the spectral function evolution of vector mesons to the current research program. In addition, CBM will measure the in-medium spectral functions of short-lived vector mesons directly by their decay into dilepton pairs.

With this work we expect to pave the understanding of kaon properties in hot and dense matter and provide an essential ingredient for the ϕ-meson phenomenology in heavy-ion collisions. Our results are based on a self-consistent many-body calculation at finite temperature that relies on a realistic model of the kaon nucleon interaction thoroughly confronted to kaon nuclear phenomenology.

ACKNOWLEDGMENTS

We thank E. Oset for useful discussions. We also thank R. Rapp for helpful discussions and comments at the initial stage of the project. This work is partly supported by the EU contract FLAVIAnet MRTN-CT-2006-035482, by the contract FIS2005-03142 from MEC (Spain) and FEDER, and by the Generalitat de Catalunya contract 2005SGR-00343. This research is part of the EU Integrated Infrastructure Initiative Hadron Physics Project under contract number RII3-CT-2004-506078. L.T. acknowledges support from the BMBF project "Hadronisierung des QGP und dynamik von hadronen mit charm quarks" (ANBest-P and BNBest-BMBF 98/NKBF98). D.C. acknowledges support from the "Juan de la Cierva" Programme (Ministerio de Educación y Ciencia, Spain).

APPENDIX A: FINITE-TEMPERATURE LINDHARD FUNCTIONS

We quote here some Lindhard function expressions in the ITF to point out the main differences with previous evaluations.

A. YN^{-1} excitations

In the ITF, the YN^{-1} Lindhard function reads

$$\mathcal{U}_{YN^{-1}}(\omega_n, \vec{q}; T) = 2 \int \frac{d^3p}{(2\pi)^3} \frac{n_N(\vec{p}, T) - n_Y(\vec{p}+\vec{q}, T)}{\mathrm{i}\omega_n + E_N(\vec{p}, T) - E_Y(\vec{p}+\vec{q}, T)}, \quad \text{(A1)}$$

where ω_n is a bosonic Matsubara frequency ($\mathrm{i}\omega_n = \mathrm{i}2n\pi T$) and the factor 2 stands for spin degeneracy. Consistently with the approximations employed in this work, we have kept only the positive energy part of the baryon propagators, while keeping the baryon energies fully relativistic and containing also mean-field binding potentials. The nucleon and hyperon Fermi distributions, $n_{N,Y}(\vec{p}, T) = [e^{(E_{N,Y}(\vec{p},T)-\mu_B)/T} + 1]^{-1}$, depend on the temperature and baryon chemical potential, so for fixed T and μ_B the nucleon and hyperon densities are given by

$$\rho_N = \nu_N \int \frac{d^3p}{(2\pi)^3} n_N(\vec{p}, T), \qquad \rho_Y = \nu_Y \int \frac{d^3p}{(2\pi)^3} n_Y(\vec{p}, T), \quad \text{(A2)}$$

with ν_B the corresponding spin-isospin degeneracy factors, namely $\nu_N = 4$ and $\nu_Y = (2, 6, 12)$ for $Y = (\Lambda, \Sigma, \Sigma^*)$. All the hyperons are considered as stable particles.

Note that, in contrast to the zero temperature case shown below, at finite temperature there are occupied hyperon states and therefore the Yh excitation is suppressed by hyperon Pauli blocking, as it is evident from the hyperon distribution, n_Y, which appears as a subtraction in the numerator of the Lindhard function. This can be seen explicitly by rewriting $n_N - n_Y$ as $n_N(1 + n_Y) - n_Y(1 + n_N)$.

Analytical continuation to real energies ($\mathrm{i}\omega_n \to q_0 + \mathrm{i}\varepsilon$) gives the following expressions for the real and imaginary parts of the finite temperature YN^{-1} Lindhard function (including mean-field binding potentials),

$$\mathrm{Re}U_{YN^{-1}}(q_0, \vec{q}; T) = \frac{1}{2\pi^2} \int_0^\infty dp\, p^2 \times \mathcal{P} \int_{-1}^{+1} du \frac{n_N(\vec{q}, T) - n_Y(\vec{p}+\vec{q}, T)}{q_0 + E_N(\vec{p}, T) - E_Y(\vec{p}+\vec{q}, T)},$$

$$\begin{aligned}&\mathrm{Im}U_{YN^{-1}}(q_0,\vec{q};T)\\&=-\pi\,\frac{1}{2\pi^2}\int_0^\infty dpp^2\,\frac{q_0+E_N(\vec{p},T)-\Sigma_Y}{p\,q}\\&\times[n_N(\vec{q},T)-n_Y(\vec{p}+\vec{q},T)]_{u_0}\\&\times\theta(1-|u_0|)\theta(q_0+E_N(\vec{p},T)-\Sigma_Y),\end{aligned}\tag{A3}$$

with $u_0\equiv u_0(q_0,q,p)=[(q_0+E_N-\Sigma_Y)^2-(M_Y^*)^2-p^2-q^2]/(2\,p\,q)$, where here q, p refer to the modulus of the corresponding three-momentum.

In the limit of zero temperature and fixed baryon chemical potential, μ_B, which then coincides with the nucleon Fermi energy, $E_F=E_N(p_F)$, with p_F the Fermi momentum, we have

$$n_N(\vec{p},T)\to n_N(\vec{p})=\theta(p_F-p)\,,n_Y(\vec{p},T)\to 0.\tag{A4}$$

The YN^{-1} Lindhard function then reads

$$\begin{aligned}&U_{YN^{-1}}(q_0,\vec{q};\rho)\\&=2\int\frac{d^3p}{(2\pi)^3}\,\frac{n_N(\vec{p})}{q_0+E_N(\vec{p})-E_Y(\vec{p}+\vec{q})+\mathrm{i}\varepsilon},\end{aligned}\tag{A5}$$

and $\rho=2p_F^3/3\pi^2$. In Refs. [10,45,46] analytical expressions are provided for the nonrelativistic Fermi gas [i.e., $E_B(\vec{p})=M_B+\vec{p}^{\,2}/2M_B$ above], which we quote here for completeness,

$$\begin{aligned}&\mathrm{Re}U^{\mathrm{nr}}_{YN^{-1}}(q_0,\vec{q};\rho)=\frac{3}{2}\rho\frac{M_Y}{qp_F}\left[z+\frac{1}{2}(1-z^2)\ln\frac{|z+1|}{|z-1|}\right],\\&\mathrm{Im}U^{\mathrm{nr}}_{YN^{-1}}(q_0,\vec{q};\rho)=-\frac{3}{4}\pi\rho\frac{M_Y}{qp_F}[(1-z^2)\theta(1-|z|)],\end{aligned}\tag{A6}$$

with

$$z=\frac{M_Y}{qp_F}\left[q_0-\frac{\vec{q}^{\,2}}{2M_Y}-(M_Y-M_N)\right].\tag{A7}$$

We note that terms proportional to $(M_Y^{-1}-M_B^{-1})$ in the denominator of Eq. (A5) are neglected when doing the angular integration to arrive at Eq. (A6).

In the literature, one often finds approximate expressions for the finite temperature Lindhard function that have been obtained from extensions of the former $T=0$ equations. In [10] the finite temperature generalization of Eq. (A5) was obtained by replacing the nucleon occupation number, $n_N(\vec{p})=\theta(p_F-p)$, by the corresponding Fermi distribution at finite temperature, $n_N(\vec{p})\to n_N(\vec{p},T)$. Analytical expressions (up to a momentum integration) read

$$\begin{aligned}&\mathrm{Re}U^{\mathrm{nr}}_{YN^{-1}}(q_0,\vec{q};T)=\frac{1}{\pi^2}\frac{M_Y}{q}\int dp\,p\,n_N(\vec{p},T)\ln\frac{|z+1|}{|z-1|},\\&\mathrm{Im}U^{\mathrm{nr}}_{YN^{-1}}(q_0,\vec{q};T)=-\frac{1}{\pi}T\frac{M_NM_Y}{q}\ln\frac{1}{1-n_N(\vec{p}_m,T)},\end{aligned}\tag{A8}$$

with

$$\begin{aligned}z&=\frac{M_Y}{qp}\left[q_0-\frac{\vec{q}^{\,2}}{2M_Y}-(M_Y-M_N)\right],\\p_m&=\frac{M_Y}{q}\left|q_0-(M_Y-M_N)-\frac{\vec{q}^{\,2}}{2M_Y}\right|.\end{aligned}\tag{A9}$$

B. ph and Δh excitations

The evaluation of the ph $\equiv NN^{-1}$ Lindhard function at finite temperature and density can be found, for instance, in Refs. [75,91]. Analytical continuation to real energies from the ITF expression leads to

$$\begin{aligned}&U_{NN^{-1}}(q_0,\vec{q};T)\\&=\nu_N\int\frac{d^3p}{(2\pi)^3}\,\frac{n_N(\vec{p},T)-n_N(\vec{p}+\vec{q},T)}{q_0+\mathrm{i}\varepsilon+E_N(\vec{p},T)-E_N(\vec{p}+\vec{q},T)},\end{aligned}\tag{A10}$$

with $\nu_N=4$. Similarly, for the Δh Lindhard function we arrive at

$$\begin{aligned}&U_{\Delta N^{-1}}(q_0,\vec{q};T)\\&=\nu_\Delta\int\frac{d^3p}{(2\pi)^3}\\&\times\left[\frac{n_N(\vec{p},T)-n_\Delta(\vec{p}+\vec{q},T)}{q_0+\mathrm{i}\frac{\Gamma_\Delta(q_0,\vec{q})}{2}+E_N(\vec{p},T)-E_\Delta(\vec{p}+\vec{q},T)}\right.\\&\left.+\,\frac{n_\Delta(\vec{p},T)-n_N(\vec{p}+\vec{q},T)}{q_0+\mathrm{i}\frac{\Gamma_\Delta(-q_0,\vec{q})}{2}+E_\Delta(\vec{p},T)-E_N(\vec{p}+\vec{q},T)}\right],\end{aligned}\tag{A11}$$

which we have written explicitly in terms of direct (ΔN^{-1}) plus crossed ($N\Delta^{-1}$) contributions. For convenience, the $\pi N\Delta$ coupling is absorbed in the definition of $U_{\Delta N^{-1}}$ and thus $\nu_\Delta=\frac{16}{9}(f_\Delta/f_N)^2$. Note that in Eq. (A11) we have accounted for the decay width of the Δ resonance. A realistic treatment of the Δh mechanism should account for the full energy-dependent Δ decay width into its dominant channel, πN. We implement the Δ decay width using the formulae in Ref. [67], in which Γ_Δ depends only on the pion energy and momentum (a more detailed study of the in-medium Δ self-energy at finite temperature and density was reported in Ref. [92]). $\Gamma_\Delta(q_0,\vec{q})$ accounts for both direct and crossed kinematics and hence the retarded property of $U_{\Delta N^{-1}}$ is preserved. We have not accounted for binding effects on the nucleon and Δ in the pion self-energy. First, in the ph excitation the baryonic potentials cancel to a large extent. Second, the binding potentials for the Δ resonance are not well known experimentally and we omit them. Therefore, for consistence, we do not dress the nucleon in the Δh excitation either.

The $T\to 0$ limit (at nuclear matter conditions) of $U_{NN^{-1}}$ and $U_{\Delta N^{-1}}$ can be easily obtained with similar prescriptions as in the YN^{-1} case, namely $n_N(\vec{p},T)\to n_N(\vec{p})$ and $n_\Delta\to 0$. Analytic expressions for the nonrelativistic ph and Δh Lindhard functions can be found in Ref. [67].

APPENDIX B: s-WAVE SELF-ENERGY FROM $T_{\bar{K}(K)N}$

We derive in this section a general expression for the contribution to the kaon self-energy from the effective in-medium $\bar{K}(K)N$ scattering amplitude at finite temperature. Let us denote by $T_{\bar{K}(K)N}$ the isospin averaged kaon nucleon scattering amplitude. The kaon self-energy, $\Pi_{\bar{K}(K)N}$, follows from closing the nucleon external lines and, following the

Feynman rules in the ITF, reads

$$\Pi_{\bar{K}(K)N}(\omega_n,\vec{q};T) = T\sum_{m=-\infty}^{\infty}\int\frac{d^3p}{(2\pi)^3}\frac{1}{\mathrm{i}W_m - E_N(\vec{p})} \times T_{\bar{K}(K)N}(\omega_n + W_m,\vec{P};T), \quad \text{(B1)}$$

where ω_n and W_m are bosonic and fermionic Matsubara frequencies, respectively, $\mathrm{i}\omega_n = \mathrm{i}2n\pi T$ and $\mathrm{i}W_m = \mathrm{i}(2m+1)\pi T + \mu_B$. The sum over the index m is not straightforward because $T_{\bar{K}(K)N}$ depends on m in a nontrivial way. To skip this complication, we can invoke a spectral representation for the T matrix (inherited from the analytical structure of the meson-baryon loop function) and we have

$$\begin{aligned}\Pi_{\bar{K}(K)N}(\omega_n,\vec{q};T) &= -T\sum_{m=-\infty}^{\infty}\int\frac{d^3p}{(2\pi)^3}\frac{1}{\pi}\int_{-\infty}^{\infty}d\Omega \times\frac{\mathrm{Im}\,T_{\bar{K}(K)N}(\Omega,\vec{P};T)}{[\mathrm{i}W_m - E_N(\vec{p})][\mathrm{i}\omega_n + \mathrm{i}W_m - \Omega]} \\ &= -\int\frac{d^3p}{(2\pi)^3}\frac{1}{\pi}\int_{-\infty}^{\infty}d\Omega\frac{\mathrm{Im}\,T_{\bar{K}(K)N}(\Omega,\vec{P};T)}{\mathrm{i}\omega_n - \Omega + E_N(\vec{p})} \times[n_N(\vec{p},T) - n(\Omega,T)], \quad \text{(B2)}\end{aligned}$$

with $n(\Omega,T) = [e^{(\Omega-\mu_B)/T}+1]^{-1}$ here. The former result, after continuation into the real energy axis ($\mathrm{i}\omega_n \to q_0 + \mathrm{i}\varepsilon$), provides the thermal kaon self-energy evaluated from the kaon nucleon scattering amplitude. Note that it includes a Pauli-blocking correction term, $n(\Omega,T)$, convoluted with the spectral strength from the imaginary part of the T matrix. At the region in which the principal value of the spectral integration gets its major contribution, $\Omega \approx q_0 + E_N(\vec{p})$, the fermion distribution $n(\Omega,T)$ behaves as a slowly varying exponential tail (for the present temperatures under study). We can approximate this term by a constant, namely $n(\Omega,T) \simeq n(q_0 + E_N(\vec{p}),T)$, and take it out of the integral. The dispersion integral over Ω then recovers the full amplitude $T_{\bar{K}(K)N}$ and the self-energy can be approximated by:

$$\Pi_{\bar{K}(K)N}(q_0 + \mathrm{i}\varepsilon,\vec{q};T) = \int\frac{d^3p}{(2\pi)^3}T_{\bar{K}(K)N}(q_0 + E_N(\vec{p}),\vec{P};T) \times[n_N(\vec{p},T) - n(q_0 + E_N(\vec{p}),T)]. \quad \text{(B3)}$$

Note that this procedure is exact for the imaginary part. Equation (24) follows from the former result by neglecting the Pauli-blocking correction on the fermion degrees of freedom excited in the kaon nucleon amplitude (note that in the isospin zero amplitude the strength peaks around the $\Lambda(1405)$ resonance, and thus one expects this correction to be small with respect to that on the nucleon).

[1] E. Friedman and A. Gal, Phys. Rep. **452**, 89 (2007).
[2] R. Rapp and J. Wambach, Adv. Nucl. Phys. **25**, 1 (2000).
[3] C. Fuchs, Prog. Part. Nucl. Phys. **56**, 1 (2006).
[4] V. Koch, Phys. Lett. **B337**, 7 (1994).
[5] J. Schaffner-Bielich, V. Koch, and M. Effenberger, Nucl. Phys. **A669**, 153 (2000).
[6] M. Lutz, Phys. Lett. **B426**, 12 (1998).
[7] M. F. M. Lutz and C. L. Korpa, Nucl. Phys. **A700**, 309 (2002).
[8] A. Ramos and E. Oset, Nucl. Phys. **A671**, 481 (2000).
[9] L. Tolos, A. Ramos, A. Polls, and T. T. S. Kuo, Nucl. Phys. **A690**, 547 (2001).
[10] L. Tolos, A. Ramos, and A. Polls, Phys. Rev. C **65**, 054907 (2002).
[11] L. Tolos, A. Ramos, and E. Oset, Phys. Rev. C **74**, 015203 (2006).
[12] C. J. Batty, E. Friedman, and A. Gal, Phys. Rep. **287**, 385 (1997).
[13] A. Baca, C. Garcia-Recio, and J. Nieves, Nucl. Phys. **A673**, 335 (2000).
[14] Y. Akaishi and T. Yamazaki, Phys. Rev. C **65**, 044005 (2002).
[15] A. Dote, H. Horiuchi, Y. Akaishi, and T. Yamazaki, Phys. Rev. C **70**, 044313 (2004).
[16] Y. Akaishi, A. Dote, and T. Yamazaki, Phys. Lett. **B613**, 140 (2005).
[17] E. Oset and H. Toki, Phys. Rev. C **74**, 015207 (2006).
[18] T. Suzuki *et al.*, Phys. Lett. **B597**, 263 (2004).
[19] M. Sato *et al.*, Phys. Lett. **B659**, 107 (2008); M. Iwasaki *et al.*, Nucl. Phys. **A804**, 186 (2008).
[20] M. Agnello *et al.* (FINUDA Collaboration), Nucl. Phys. **A775**, 35 (2006).
[21] A. Ramos, V. K. Magas, E. Oset, and H. Toki, Nucl. Phys. **A804**, 219 (2008).
[22] M. Agnello *et al.* (FINUDA Collaboration), Phys. Rev. Lett. **94**, 212303 (2005).
[23] V. K. Magas, E. Oset, A. Ramos, and H. Toki, Phys. Rev. C **74**, 025206 (2006).
[24] T. Suzuki *et al.* (KEK-PS E549 Collaboration), Phys. Rev. C **76**, 068202 (2007).
[25] M. Agnello *et al.* (FINUDA Collaboration), Phys. Lett. **B654**, 80 (2007).
[26] V. K. Magas, E. Oset, and A. Ramos, Phys. Rev. C **77**, 065210 (2008).
[27] N. V. Shevchenko, A. Gal, and J. Mares, Phys. Rev. Lett. **98**, 082301 (2007).
[28] N. V. Shevchenko, A. Gal, J. Mares, and J. Revai, Phys. Rev. C **76**, 044004 (2007).
[29] Y. Ikeda and T. Sato, Phys. Rev. C **76**, 035203 (2007).
[30] A. Doté and W. Weise, *Proceedings of the IX International Conference on Hypernuclear and Strange Particle Physics, Mainz (Germany)*, October 10–14, 2006, edited by J. Pochodzalla and Th. Walcher (Springer, Germany, 2007), p. 249; A. Doté, T. Hyodo, and W. Weise, Nucl. Phys. **A804**, 197 (2008).
[31] A. Forster *et al.*, Phys. Rev. C **75**, 024906 (2007).
[32] http://www.gsi.de/forschung/kp/kp1/experimente/fopi/index.html.
[33] W. Cassing, L. Tolos, E. L. Bratkovskaya, and A. Ramos, Nucl. Phys. **A727**, 59 (2003).
[34] L. Tolos, D. Cabrera, A. Ramos, and A. Polls, Phys. Lett. **B632**, 219 (2006).

[35] Y. Akiba *et al*. (E-802 Collaboration), Phys. Rev. Lett. **76**, 2021 (1996).
[36] S. S. Adler *et al*. (PHENIX Collaboration), Phys. Rev. C **72**, 014903 (2005).
[37] D. Adamova *et al*. (CERES Collaboration), Phys. Rev. Lett. **96**, 152301 (2006).
[38] T. Ishikawa *et al*., Phys. Lett. **B608**, 215 (2005).
[39] R. Muto *et al*., Nucl. Phys. **A774**, 723 (2006).
[40] R. Nasseripour *et al*. (CLAS Collaboration), Phys. Rev. Lett. **99**, 262302 (2007).
[41] T. Hatsuda and S. H. Lee, Phys. Rev. C **46**, R34 (1992).
[42] M. Asakawa and C. M. Ko, Nucl. Phys. **A572**, 732 (1994).
[43] S. Zschocke, O. P. Pavlenko, and B. Kampfer, Eur. Phys. J. A **15**, 529 (2002).
[44] F. Klingl, T. Waas, and W. Weise, Phys. Lett. **B431**, 254 (1998).
[45] E. Oset and A. Ramos, Nucl. Phys. **A679**, 616 (2001).
[46] D. Cabrera and M. J. Vicente Vacas, Phys. Rev. C **67**, 045203 (2003).
[47] W. Smith and K. L. Haglin, Phys. Rev. C **57**, 1449 (1998).
[48] L. Alvarez-Ruso and V. Koch, Phys. Rev. C **65**, 054901 (2002).
[49] D. Cabrera, L. Roca, E. Oset, H. Toki, and M. J. Vicente Vacas, Nucl. Phys. **A733**, 130 (2004).
[50] R. Arnaldi *et al*. (NA60 Collaboration), Phys. Rev. Lett. **96**, 162302 (2006).
[51] http://www-hades.gsi.de.
[52] http://www.gsi.de/fair/experiments/CBM/.
[53] L. Tolos, A. Ramos, and T. Mizutani, Phys. Rev. C **77**, 015207 (2008).
[54] E. Oset and A. Ramos, Nucl. Phys. **A635**, 99 (1998).
[55] J. Gasser and H. Leutwyler, Nucl. Phys. **B250**, 465 (1985).
[56] U. G. Meissner, Rep. Prog. Phys. **56**, 903 (1993).
[57] V. Bernard, N. Kaiser, and U. G. Meissner, Int. J. Mod. Phys. E **4**, 193 (1995).
[58] A. Pich, Rep. Prog. Phys. **58**, 563 (1995).
[59] G. Ecker, Prog. Part. Nucl. Phys. **35**, 1 (1995).
[60] D. Jido, J. A. Oller, E. Oset, A. Ramos, and U. G. Meissner, Nucl. Phys. **A725**, 181 (2003).
[61] J. A. Oller and E. Oset, Phys. Rev. D **60**, 074023 (1999).
[62] J. A. Oller and U. G. Meissner, Phys. Lett. **B500**, 263 (2001).
[63] J. I. Kapusta and C. Gale, *Finite Temperature Field Theory Principles and Applications*, 2nd ed. (Cambridge University Press, New York, 2006).
[64] R. Machleidt, Adv. Nucl. Phys. **19**, 189 (1989).
[65] K. Tsushima and F. C. Khanna, Phys. Lett. **B552**, 138 (2003).
[66] K. Tsushima and F. C. Khanna, J. Phys. G **30**, 1765 (2004).
[67] E. Oset, P. Fernandez de Cordoba, L. L. Salcedo, and R. Brockmann, Phys. Rep. **188**, 79 (1990).
[68] A. Ramos, E. Oset, and L. L. Salcedo, Phys. Rev. C **50**, 2314 (1994).
[69] T. Waas, N. Kaiser, and W. Weise, Phys. Lett. **B379**, 34 (1996).
[70] T. Waas and W. Weise, Nucl. Phys. **A625**, 287 (1997).
[71] C. Garcia-Recio, J. Nieves, T. Inoue, and E. Oset, Phys. Lett. **B550**, 47 (2002).
[72] E. Oset, H. Toki, and W. Weise, Phys. Rep. **83**, 281 (1982).
[73] R. Seki and K. Masutani, Phys. Rev. C **27**, 2799 (1983).
[74] O. Meirav, E. Friedman, R. R. Johnson, R. Olszewski, and P. Weber, Phys. Rev. C **40**, 843 (1989).
[75] M. Urban, M. Buballa, R. Rapp, and J. Wambach, Nucl. Phys. **A673**, 357 (2000).
[76] C. Garcia-Recio, J. Nieves, E. Ruiz Arriola, and M. J. Vicente Vacas, Phys. Rev. D **67**, 076009 (2003).
[77] D. Jido, A. Hosaka, J. C. Nacher, E. Oset, and A. Ramos, Phys. Rev. C **66**, 025203 (2002).
[78] C. Garcia-Recio, M. F. M. Lutz, and J. Nieves, Phys. Lett. **B582**, 49 (2004).
[79] S. M. Flatte, Phys. Lett. **B63**, 224 (1976).
[80] M. F. M. Lutz, C. L. Korpa, and M. Moller, Nucl. Phys. **A808**, 124 (2008).
[81] A. Mangiarotti *et al*., Nucl. Phys. **A714**, 89 (2003).
[82] C. L. Korpa and M. F. M. Lutz, Heavy Ion Phys. **17**, 341 (2003).
[83] M. Nekipelov *et al*., Phys. Lett. **B540**, 207 (2002).
[84] C. Gale and J. I. Kapusta, Nucl. Phys. **B357**, 65 (1991).
[85] K. L. Haglin and C. Gale, Nucl. Phys. **B421**, 613 (1994).
[86] R. Rapp, Phys. Rev. C **63**, 054907 (2001).
[87] L. Holt and K. Haglin, J. Phys. G **31**, S245 (2005).
[88] B. V. Martemyanov, A. Faessler, C. Fuchs, and M. I. Krivoruchenko, Phys. Rev. Lett. **93**, 052301 (2004).
[89] E. Santini, G. Burau, A. Faessler, and C. Fuchs, Eur. Phys. J. A **28**, 187 (2006).
[90] D. Cabrera and L. Tolós (in preparation).
[91] R. D. Mattuck, *A Guide to Feynman Diagrams in the Many Body Problem*, 2nd ed. (Dover, New York, 2002).
[92] H. van Hees and R. Rapp, Phys. Lett. **B606**, 59 (2005).